Author’s response to Reviewer #1

We thank Reviewer #1 for their detailed comments and suggestions for improving the manuscript. We addressed their comments as follows:

Comment: *page 6, line 34: The details of the zero air inlet design are quite crucial for the success of the proposed HFA method. However, unlike stated in this sentence, no corresponding details are visible in Fig. 1. The authors should give a close-up view of the gas inlet and the attached inlet for the zero gas. In addition it needs to be specified, how the zero gas unit (heating catalyst) was operated during periods of normal EC measurements (outside the zeroing periods).*

Response: We included a close-up view of the inlet piece in Fig. 1. Since we used a slightly different glass inlet as compared to Ellis et al. (2010), the zero air was introduced through a PFA T-fitting at the front of the inlet. Therefore, we updated this sentence in the manuscript. The heating catalyst was running continuously, where the NH_3 scrubbed air was vented into ambient air during periods of normal EC measurements. We added a note at the end of the paragraph.

Comment: *page 11, Eq. 8: The presented correction of the cospectra using sqrt[T(f)] only accounts for the damping of the fluctuation amplitudes. However a first order filter as characterised in Eqs. 5 and 6 also leads to a phase shift in the damped frequencies (e.g. Horst, 1997; Massman and Ibrom, 2008). Because the constant phase angle shift corresponds to different lag times for different frequencies, this effect is only partly compensated by the empirical lag time correction. Thus especially for HFA over a large frequency range, as observed here, the unaccounted phase shift can be important. This effect should be addressed in the manuscript.*

Response: We thank the reviewer for this comment. Indeed, the used transfer functions do not include the phase shift of a first order filter. Using a transfer function for the phase shift is complex, especially since the lag time correction accounts for some of the flux loss caused by the phase shift. Instead of applying the described transfer functions to the co-spectrum, we therefore updated the simulation method by applying a low pass filter to the 30 min time series in the time domain and subsequently performing a cross-correlation analysis to account for the lag time shift as it is done with the real flux data. Using this approach, both the effect of the phase shift and the lag time correction are accounted for. Using this new approach in the flux loss simulation, we updated Fig. 9 and the empirical relationship between the flux attenuation factor and the *D* value (Fig. 10 and Eq. 12 in the revised manuscript). As a result of the updated flux correction, fluxes increased by a further 25 % (median value) over the corrected values presented in the original manuscript. Final flux values were updated accordingly in the entire manuscript. The method section 2.4.2 was updated using the time domain approach. Since the calculation of the transfer function is not necessarily needed with the time domain approach, the method was renamed to “time response method” in the entire manuscript. The description of results in Sect. 3.2.3 was also updated accordingly.

Comment: *Page 19, line 5-6: Concerning the results of the ogive method, it is stated here that the results from least-squares regression (corresponding to an arithmetic averaging) strongly deviated from the median. This is not surprising because the ogive results represent ratios of (very noisy) half-hourly cospectra. Such data usually have a non-Gaussian (non-symmetric) distribution. Therefore the application of a simple least-squares regression in Fig. 6 is not adequate. Instead, the calculation of binned medians (as e.g. used in Fig. 8) or a median regression would be much more suitable (eventually with separation of stable and unstable cases). In that way, a dependence on windspeed possibly could be detected. Also for the analysis of the temporal behavior (before/after inlet cleaning) a running median filter should be applied to the ogive data. Generally: if two approaches for HFA are inter-compared and rated, they should both be evaluated in an adequate and careful way. Thus the evaluation of the ogive method needs to be improved as suggested.*

Response: We agree that using binned median or a median regression could be more adequate for interpreting the ogive results. We therefore updated Fig. 6 showing the box plot statistics of the flux attenuation factor against binned wind speed data. We then used a quartile (median) regression to retrieve the linear relationship against wind speed. Using this approach the dependency of the attenuation factor on the wind speed is slightly stronger (factor of -0.033 instead of -0.028). We updated the coefficients in Eq. 11 (of revised manuscript) and its description. Still, the similarity of the new linear regression coefficients with previously used coefficients supports our finding that the flux attenuation determined with the ogive method is less than with the proposed time response method.

Comment: *page 8, line 3-6: With respect to its potential influence on the HFA, it would be of interest to show (or quantitatively describe) the temporal variations of observed lag times.*

Response: After (1) synchronizing the two data acquisition systems and (2) applying the described quality control, the standard deviation of the lag time between the NH_3 mixing ratio and the vertical wind speed measurements was 1.1 s. Since a larger HFA leads to a flatter cross-correlation peak, a larger variation of the time lag during times with high D values would be expected. However, this could not be observed. Therefore, we think that the variations in the lag time are dominated by other factors. For example, part of the variation (about 0.5 s) can be explained by changes in the wind speed influencing the lag time between the sonic anemometer and inlet position. We added a description on the variation of the lag time in the manuscript.

Comment: *page 9, line 21: How stable was the 'background' signal (y_0) of the QCL during the study? Its variability would be an indication for the systematic uncertainty and the total accuracy of the QCL measurements.*

Response: We agree that a stable operation of the QCL is crucial for reliable and accurate QCL measurements. However, as described in the methods section, during the operation of QCL the automated background schedule was activated, which already accounts for the drift and is a common procedure for QCL measurements. This procedure is enabled to maximize the accuracy, given that used zero air is free of NH_3. To correct for a potential drift of the QCL between two automated background periods, the background mixing ratios were linearly interpolated between two consecutive background measurements and subtracted from the NH_3 mixing ratios. Due to the precise temperature control the QCL was generally running in a very stable way. As a result, even during the periods when automated backgrounds were collected only every three hours, the drift was typically less than 0.3 ppbv over the three hour period.

Comment: *page 10, Eq. 7: The representation of the two different response times (exp. functions) by the combined transfer function in Eq. 7 yields an adequate result in practice for the present study. However, the additive combination of individual transfer functions is conceptually problematic. It e.g. implies that the fast* τ_1 *filter only acts on a fraction (1-D) of the concentration fluctuations. However, if this filter (as suggested by the authors) can be attributed to the air mixing in the analyser detection cell, it physically acts on all fluctuations. Therefore, a multiplicative combination of the transfer functions would be conceptually more adequate in my view, and it would be compatible to the classical transfer function method (Moore, 1986; Moncrieff et al., 1997). At least the relation and differences between additive vs. multiplicative combination of transfer functions should be discussed.*

Response: We agree with the reviewer that a multiplicative combination would be conceptually more adequate, however only if both τ_1 and τ_2 are determined independently. In our analysis, both τ_1 and τ_2 were determined using the double exponential decay function from the time response. Since they are linked by the D value they are not independent from each other. While τ_1 can be estimated by the sample cell (+sample tube) volume, pressure and flow rate, we cannot determine τ_2 from the time response measurements independently from τ_1. Therefore, using the double exponential time response model as a concept, we find that the presented additive approach is more appropriate in defining a combined transfer function.

Note: In the updated manuscript we applied the low-pass filter in the time domain instead of using transfer function (in reaction to comment above on phase shift). The filters for τ_1 and τ_2 were still combined additively and scaled by the D value.

Comment: *Although the focus of this study is the HFA method, it would be suitable to give information about the possible sources of* NH_3 *in May and August (Fig. 3) as a difference to other months showing deposition. Therefore, the timing, type and amount of fertilizer applications to the corn field (before or during measurement period) should be reported.*

Response: The plausibility of measured fluxes is important for the presented technical paper, which is why we addressed this in more detail in the answer to the comment of Neftel & Hensen and added a paragraph on the plausibility of NH_3 fluxes in Section 4.3.2. Due to the complexity of the bi-directional exchange of NH_3, it is out of the scope of this paper to discuss the underlying processes of NH_3 in more detail, but will be discussed in a subsequent paper under preparation by the authors. Information on the fertilization time (25 May), type (granular urea) and amount (155 kg N ha^{-1}) are given in Sect. 2.1.2.

Comment: *In order to decide whether the estimated flux detection limit (closely related to the flux uncertainty) is plausible, some exemplary time series with measured half-hourly fluxes should be presented. These would be more informative in the present context than the statistical diurnal cycles in Fig. 3.*

Response: We showed the statistical diurnal cycles instead of an exemplary time series to give an overview of the variable magnitude and direction NH_3 fluxes over the growing season in relation to the flux detection limit. In our opinion, this gives a better overview of the performance of the eddy covariance system and quality of the flux measurements than a selected time series. However, we agree that the shown flux boxplot statistics are not ideal for the comparison with the median flux detection limit since they combine values from both positive and negative fluxes. We therefore updated Fig. 3 and its description in Sect. 3.1 using the absolute NH_3 flux values for the boxplot statistics, while the percentages of flux periods with emission or deposition are given for each month. Furthermore, to make clear that the shown fluxes are before the application of the HFA correction, we additionally indicated this in the title of Sect. 3.1.

Comment: *page 11, line 24: This precision only represents the precision at zero concentration while the precision at higher ambient concentrations could be larger. This should be specified.*

Response: The precision over the course of the experiment was determined from the zero air measurements. We found that the precision of the NH_3 QCL does not change at higher NH_3 mixing ratios. This was tested by applying a known constant NH_3 mixing ratio (~8 ppbv) through the calibration port of the glass inlet. We added a note that the precision was independent of the measured NH_3 mixing ratio.

Comment: *A separate quantification of the HFA factor with the τ_1 transfer function alone would be of interest in order to partition the total damping into 'classical' damping effects applicable to all trace gases and wall sorption effects only applicable to NH_3.*

Response: This case, where only τ_1 is responsible for the HFA, is considered in the case of $D = 0$. Hence, in Eq. 12 (of revised manuscript) the damping that is not due to the wall effects and applicable also to other trace gases is described by "$\alpha_{tr} = -0.47 \cdot u + 0.93$". We added a note explaining this in Sect. 3.2.3.

Comment: *page 13, lines 6-7: Were the distinct temporal variations in D found only after fixing τ_1 and τ_2 to overall constant values, or were they equally found with variable τ_1 and τ_2?*

Response: Thank you for asking this question. τ_1 and τ_2 were only fixed for the HFA simulation (Sect. 3.2.3). The shown temporal variation of D was retrieved without fixing τ_1 and τ_2 in Eq. 2 (Sect 2.3). However, we tested this and found that fixing τ_1 and τ_2 to the median values resulted in a comparable temporal variation of the D value.

Comment: *page 13, lines 17-18: In my view the dependence of the D value from the NH_3 concentration in Figure 8 is not so clear as stated in this sentence. To get a better impression from Fig. 8, it would be useful to indicate the number of data (n) in each bin.*

Response: In Fig. 8 we included the number of data points used in each bin. As one might suspect, there are less data points at high NH_3 mixing ratios where the variation is less. The larger uncertainty of the double exponential fit with small mixing ratio changes may be the cause of the observed larger variation of D values at lower mixing ratios, as we had noted in the text of the manuscript.

Comment: *page 13, line 26: "time constants were fairly constant over time" is a strange statement. I suggest to replace "time constants" by "response times".*

Response: We improved the wording of this sentence. We prefer to use the term “time constant” since it has a more accurate definition, namely the time required for the NH_3 measurement to respond to 63.2 % of its final value.

Comment: *Figure 7: What was the reason for the decrease and subsequent increase of D at the end of August?*

Response: From 23 to 28 August, the D value was decreasing, which is against the increasing trend of D over the month of August. We were not able to determine a specific reason for the temporary decline and subsequent increase. Possible is a change in ambient air characteristics that would influence the wall interaction. However, the fact that we cannot attribute a single factor (such as NH_3 ambient mixing ratios, humidity, temperature or operational changes) to the change in time response, shows the complexity of NH_3 time response. This is also one important reason, why we conclude in the paper that using an experimental approach like the time response method is necessary to adequately correct the high frequency attenuation of NH_3 eddy covariance fluxes.

Author’s response to Reviewer #2

We thank Reviewer #2 for their overall positive feedback on our manuscript. We addressed their comments as follows:

***Comment**: Page 2, Line 5: In addition to Europe, the Great Salt Lake Region also experienced an ammonium salts rich condition, as suggested by another paper of the authors (Moravek et al., 2019). This is also the case in North China (Li et al., 2019). It is better to mention this worldwide situation here.*

Response: We mention Europe here, since Pozzer et al. (2017) found for Europe the highest PM2.5 reduction when reducing ammonia emissions on continental scale (maximum of 34 % compared to 16 % for North America and 13 % for East Asia). However, we agree with the reviewer that ammonium containing aerosols do comprise large portions of PM2.5 in many other regions as well. We therefore added a note on the more regional importance of ammonium aerosols, including the references the reviewer suggested.

***Comment:** Page 2, Lines 7-10: The major sources of ammonia are from agriculture globally and regionally. On an urban scale, however, the sources may be non-agricultural emissions (Pan et al., 2016). So the mitigation strategy for improving air quality may be not work if only controlling agricultural sources. Although I agree with the authors that measuring the flux is critical to reduce uncertainty of the ammonia inventory, identifying the major sources is also important.*

Response: We agree that identifying the major NH_3 sources is essential as well. To give a more complete picture on possible NH_3 sources, we added a sentence on the fossil-fuel based NH_3 emissions.

***Comment:** Page 2, Lines 14-15: Classic references may be required here for the readers’ convenience, rather than shown them together at lines 18-19.*

Response: Since not all references on the eddy covariance method report successful flux measurements, we found it is better to mention them in the respective section below, rather listing them here in the first sentence of the paragraph. Consequently, we listed the references for the gradient and REA method also below at lines 18-19. We found grouping them together was the best way to give an overview on the performed gradient and REA studies.

***Comment:** Page 2, Line 16: change ammonia to* NH_3*.*

Response: We made the requested change.

***Comment:** Page 4, Line 2: change particulate matter to PM, as defined at Page 2 Line 5.*

Response: Since “particulate matter” is only used three time in the manuscript, we removed the acronym definition on page 2.

Comment: *Page 4, Line 7: Just a comment, 5.5 m may be too long for ammonia determination.*

Response: The intake line for ammonia measurements should be kept as short as possible to reduce wall interactions. 5.5 m was the minimal inlet length we could use for our setup to ensure the stable operation of the QCL and optimal location of the sonic anemometer. In this paper we evaluate the effect of the wall interaction on the high frequency NH_3 measurements and show that NH_3 can be measured with a sufficiently high time response to obtain NH3 fluxes.

Comment: *Page 4, Line 7: Heated to 40 °C?*

Response: Since the information on the heating temperature is given in the method section, we think it is sufficient to mention it there.

Comment: *Page 6: Did the authors perform calibration of ammonia with known concentrations?*

Response: Since the shape of NH_3 absorption line is known from the HITRAN database, the ammonia mixing ratio can be derived directly by fitting it to the absorption spectrum measured by the QCL using sample cell pressure. The measurement therefore represents an absolute measurement technique, which does not require a calibration to obtain the NH_3 mixing ratio. Still quality checks with a known NH_3 calibration source are advisable, also to exclude potential systematic effects of the inlet system. We intended to use a continuously running NH_3 permeation oven for this, however due to problems with its stability (mixing ratios varied by ~20 %) we could not use the results. Instead the QCL measurements was compared to manual denuder measurements made at the QCL inlet, where we found an agreement of 15%.

Comment: *Page 7, Line 26: change ammonia to NH_3, check through the text.*

Response: We changed ammonia to NH_3 where applicable.

Comment: *Page 11, Results: I suggest the authors detail diurnal variations of ammonia flux.*

Response: Since the scope of this manuscript is the measurement and quality control of NH_3 fluxes, we do not describe the measured fluxes here in detail. The discussion of flux magnitudes will be presented in a subsequent paper by authors. Still, in reaction to the comment made by Neftel & Hensen, we gave more details on the plausibility of measured NH_3 fluxes.

Comment: *Finally, this reviewer is wondering if an early morning pulse of ammonia flux/ concentration was observed during this campaign. And is it possible using ammonia flux determination in this study to support the ideas proposed by Wentworth et al. (2016), who are also from Jennifer's group, that dew is a night-time reservoir and morning*

Response: Since it is not in the scope of this manuscript, the detailed discussion of the fluxes and their underlying processes will be presented in a subsequent paper by the authors. This will also include the discussion of potential sources such from evaporating dew.

List of relevant changes to the manuscript

Relevant changes to the manuscript are:

1. Changed the approach for the high frequency attenuation simulation to account for the phase shift:
    - Updated method description (Sect. 2.4.2) using time domain low-pass filter approach.
    - Updated results section (Sect. 3.2.3) and Fig. 9 accordingly.
    - Updated final flux correction factors in discussion (Sect. 4.3.2), the conclusions and the abstract.
    - Renamed method to “time response method” instead of “time response transfer function method”.

2. Showing boxplot statistics of absolute NH_3 fluxes in Fig. 3 to better compare them to flux detection limits. Updated figure description in Sect. 3.1 accordingly.

3. Ogive results: Use of quantile regression of attenuation factor against wind speed. Updated Eq. 11 and Fig. 6 showing boxplot statistics of attenuation factors against the binned horizontal wind speed.

4. Presentation of WindTrax simulation results as a proof for plausibility of measured NH_3 fluxes:
    - Summary of results in the discussion (Sect. 4.3.2).
    - Detailed description of performed analysis in Supplementary Material (new).

Overview of changes made to figures:

Figure 1: Include drawings of glass inlet piece.

Figure 3: Show boxplot statistics of absolute NH_3 fluxes instead of positive and negative fluxes.

Figure 6: Show boxplot statistics of attenuation factors against the binned horizontal wind speed instead of scatter plot.

Figure 8: Include number of data points in each bin.

Figure 9: Include transfer functions from time domain low-pass filter approach (includes phase shift); updated ogives using the new approach.

Figure 10: Updated attenuation factors and the linear regressions using the results from the time domain low-pass filter approach.

Measurements and quality control of ammonia eddy covariance fluxes: A new strategy for high frequency attenuation correction

Alexander Moravek[1*], Saumya Singh[1], Elizabeth Pattey[2], Luc Pelletier[2], Jennifer G. Murphy[1]

[1]Department of Chemistry, University of Toronto, Toronto, ON, M5S 3H6, Canada
[2]Agriculture and Agri-Food Canada, Ottawa, ON, K1A 0C6, Canada
*now at: Department of Chemistry, York University, Toronto, ON, M3J 1P3, Canada

Correspondence to: Alexander Moravek (amoravek@yorku.ca)

Abstract. Measurements of the surface-atmosphere exchange of ammonia (NH_3) are necessary to study the emission and deposition processes of NH_3 from managed and natural ecosystems. The eddy covariance technique, which is the most direct method for trace gas exchange measurements at the ecosystem level, requires trace gas detection at fast sample frequency and high precision. In the past, the major limitation for measuring NH_3 eddy covariance fluxes has been the slow time response of NH_3 measurements due to NH_3 adsorption on instrument surfaces. While high frequency attenuation correction methods are used, large uncertainties in these corrections still exist mainly due to the lack of understanding of the processes that govern the time response. We measured NH_3 fluxes over a corn crop field using a quantum cascade laser spectrometer (QCL) that enables measurements of NH_3 at a 10 Hz measurement frequency. The 5 month measurement period covered a large range of environmental conditions that included both periods of NH_3 emission and deposition and allowed us to investigate the time response controlling parameters in field conditions. Without high frequency loss correction, the median daytime NH_3 flux was 8.59 ng m^{-2} s^{-1} during emission and -19.87 ng m^{-2} s^{-1} during deposition periods, with a median daytime random flux error of 1.61 ng m^{-2} s^{-1}. The overall median flux detection limit was 2.15 ng m^{-2} s^{-1}, leading to only 11.6 % of valid flux data below the detection limit. From the flux attenuation analysis we determined a median flux loss of 17 % using the ogive method. No correlations of the flux loss with environmental or analyser parameters, such as humidity or inlet aging were found, attributed to the uncertainties in the ogive method. Therefore, we propose a new method that simulates the flux loss by using the analyser time response that is determined frequently over the course of the measurement campaign. A correction that uses as a function of the horizontal wind speed and the time response is formulated which accounts for surface aging and contamination over the course of the experiment. Using this method, the median flux loss was calculated to be ~~34~~ 46 %, substantially higher than with the ogive method.

1 Introduction

Knowledge of ammonia (NH_3) exchange processes between ecosystems and the atmosphere is essential for improving our understanding of its impact on air quality, global warming, and ecosystem health. As the most abundant base in the atmosphere, NH_3 is responsible for the formation of ammonium aerosol, impairing air quality and affecting climate. For example, it is estimated that in Europe 34 % of fine particulate matter ~~(PM)~~ is directly linked to emission of ~~ammonia~~ NH_3 that generates secondary ~~PM~~ particulate matter (Pozzer et al., 2017). Ammonium aerosol is often found to be the dominant particulate matter component in areas with strong ammonia sources as was recently reported for North China and the Great Salt Lake Region (Li et al., 2019; Moravek et al., 2019). Furthermore, deposition of NH_3~~ammonia~~ has been shown to strongly impact low-nitrogen ecosystems thereby reducing biodiversity (Erisman et al., 2013).

Major sources of NH_3 to the atmosphere are emissions from agriculture, with globally 24 Tg yr^{-1} being emitted from livestock and livestock waste and 9.4 Tg yr^{-1} from synthetic fertilizer applications on agricultural fields (Paulot et al., 2014). In urban environments, fossil-fuel based NH_3 emissions can be the dominant source (Pan et al., 2016). The understanding and quantification of these emission sources is critical to propose effective NH_3 control and mitigation strategies. However, to date large uncertainties on the magnitude of NH_3 emissions exist. This is in part due to difficulties and challenges in measuring NH_3 fluxes, especially in environments where NH_3 fluxes are small and/or frequent changes between net emission and deposition are expected.

To measure NH_3 exchange at the ecosystem level, micrometeorological methods including gradient, relaxed eddy accumulation (REA) and the eddy covariance (EC) have been used in the past. Which method is used largely depends on the expected flux magnitude, the site layout and the available instrumentation. Systems based on the capture of NH_3~~ammonia~~ by ~~wet~~ denuders or the thermal conversion to nitric oxide (NO) have been employed for flux gradient (e.g., Famulari et al., 2010; Flechard & Fowler, 1998; Sutton et al., 2000; Walker et al., 2006; Wolff et al., 2010) and REA-based flux measurements (Baum and Ham, 2009; Hansen et al., 2013, 2015; Hensen et al., 2009; Myles et al., 2007; Nelson et al., 2017; Zhu et al., 2000). The success of both methods often relies on the precise and accurate determination of a concentration difference measured over a time period of typically 30 min up to several hours. Especially under conditions where the measured vertical concentration gradient is small, like for flux measurements above forests, the REA method is the much stronger approach. The flux gradient measurement heights and the size of the REA deadband largely impact the concentration difference, and their choice has to be considered carefully in the flux measurement setup and operation (Moravek et al., 2014).

The eddy covariance method is the most direct method to quantify ecosystem scale turbulent fluxes as it relies on the covariance between the near ground turbulence and the scalar of interest. For this, the scalar has to be measured at a fast time response ($\leq$ 0.1 s) with concurrent adequately high precision. In the last two decades, the development and improvement of mass spectrometry and infrared spectroscopy techniques for fast measurements of NH_3 provided the opportunity to measure NH_3 fluxes using eddy covariance. Shaw et al. (1998) presented the first eddy covariance measurements of NH_3 using a tandem mass spectrometer and Sintermann et al. (2011) employed a proton transfer reaction mass spectrometer to measure NH_3

emissions after slurry application. For laser-based eddy covariance measurements, Famulari et al. (2004) and Whitehead et al. (2008) used diode laser absorption spectroscopy using cryogenic cooled lasers. A greater laser stability and output power is given by quantum cascade lasers (QCL) which can be Peltier-cooled (McManus et al., 2010). Ferrara et al. (2012, 2016) and Whitehead et al. (2008) used pulsed QCL spectrometers for NH_3 eddy covariance measurements on agricultural sites, while Zöll et al. (2016) employed a more sensitive continuous-wave QCL instrument to measure NH_3 fluxes above a peatland.

The common limitation of the previous studies using fast-response NH_3 analysers is the instrument time response due to the surface adsorption of NH_3. It is well-known that adsorption and desorption of NH_3 to and from surfaces, including inlet tubing, can be significant. This effect slows the time response of the measuring system leading to high frequency attenuation (HFA) of the measured NH_3 time series, which affects the NH_3 flux measurements by eddy covariance. To avoid these effects, Sun et al. (2015) employed a custom-built open-path QCL (Miller et al., 2014) to measure eddy covariance fluxes above a cattle feedlot. While open-path QCL systems have the advantage to avoid HFA effects, they may introduce flow distortion due to their size when placed close to the sonic anemometer and require frequent cleaning of the exposed cell mirrors (Sun et al., 2015). Furthermore, to our knowledge they are not commercially available yet. As closed-path systems will still play a an important role in the future, our study focuses on the performance and quality control of closed-path eddy covariance systems.

The magnitude of flux loss due to HFA in closed-path systems is highly variable depending on the instrumental setup and meteorological conditions. For past NH_3 eddy covariance field measurements, the estimated flux loss ranged between 20 and 50 % (Ferrara et al., 2012, 2016; Sintermann et al., 2011; Whitehead et al., 2008; Zöll et al., 2016). Although the flux loss can be corrected for in post-processing with spectral correction techniques, the applied correction factor can vary significantly depending on the chosen correction method (Ferrara et al., 2012). A lack of understanding of the factors impacting the time response of NH_3 eddy covariance systems is responsible for this uncertainty.

From previous studies it is known that adsorption and desorption of NH_3 is governed by the surface area and material of the inlets and internal instrument components, with stainless steel showing significantly slower time responses than polyethylene (PE) or polytetrafluoroethylene (PTFE) (Whitehead et al., 2008). Ellis et al. (2010) showed that heating of their perfluoroalkoxy (PFA) inlet tubing to 40 °C for NH_3 mixing ratios above 30 ppbv reduces the HFA significantly, while Sintermann et al. (2011) found that heating their drift tube inlet to 180 °C enabled a time resolution high enough for eddy covariance measurements. It is suspected that heating removes - at least partially - liquid and molecular water layers on the surface, which decreases the adsorption sites for the polar NH_3 molecule (Sintermann et al., 2011), although NH_3 can also interact directly with the surface material. Roscioli et al. (2015) showed that using active passivation by continuously adding a fluorinated amine into the sample gas improves the time response significantly, as the polar amine group of the molecule occupies potential NH_3 adsorption sites and NH_3 does not react with its non-polar fluoro-chain. Still, there is a lack of comprehensive mechanistic understanding of NH_3 sorption on surfaces (Sintermann et al., 2011), which is needed to reduce the uncertainties of the HFA correction for NH_3 eddy covariance fluxes. There is evidence that adsorption and desorption processes act at different rates (Whitehead et al., 2008), which would skew the high frequency NH_3 distribution and may impact the flux covariance calculation. While Ellis et al. (2010) found the time response to degrade with the relative humidity of ambient air, the potential effect on NH_3 fluxes is not accounted for in the currently used HFA flux correction methods (Ferrara et al., 2012; Zöll et al., 2016). Evidence that the time response is improved when the NH_3 mixing ratio changes are larger (Ellis et al., 2010), can be interpreted either such that fluxes with higher magnitudes need to be corrected less than small fluxes or that fluxes at higher ambient concentrations are less attenuated due to a higher passivation of the surface. Finally, the time response effect of surface aging and surface deposition of particulate matter is poorly understood and accounted for in HFA correction methods (Roscioli et al., 2015; Sintermann et al., 2011; Whitehead et al., 2008). As our understanding of NH_3 time response in changing environmental and instrumental conditions is limited, the analysis of flux datasets under a wider range of conditions than previously sampled are needed reduce the uncertainties in the HFA correction of NH_3 fluxes.

In this study, we employed a NH_3 eddy covariance system over an entire growing season from May to October 2017 at a corn field in Eastern Canada. The system used a closed-path continuous wave QCL spectrometer with a 5.5 m heated PFA inlet line. The objectives were to (1) limit adsorption/desorption of NH_3~~ammonia~~ in the inlet of the QCL; (2) quantify its impact on the systems time response under a large range of environmental and instrumental conditions in order to obtain a deeper understanding of the processes that govern the time response and of how this is ultimately applied to the NH_3 flux correction. This includes, for example, the examination of the relationship between time response and humidity or the flux magnitude. Due to the 5 month measurement period, we are able to examine the effect of inlet aging and the benefit of cleaning procedures on the NH_3 flux measurement. Based on our findings, we present an approach to correct NH_3 fluxes which uses our improved understanding of NH_3 time response. The approach may be also used for flux correction of other species that show a strong surface adsorption, such as nitric or organic acids.

Next to the issue of HFA, NH_3 measurement systems need to resolve small NH_3 mixing ratios fluctuations at high time resolution. Especially under low flux conditions, a precise and stable operation of the NH_3 measurement system is required. For this reason, the paper also discusses the precision and flux detection limit of the QCL spectrometer depending on environmental and operational conditions. Currently, continuous wave QCL spectrometers are the most precise high time resolution NH_3 measurement systems available; however, their operation under field conditions requires careful setup and regular maintenance. With our findings we provide details on the setup and operation of the QCL which are helpful for investigators that aim to use it for eddy covariance NH_3 flux measurements in the future.

2 Methods

2.1 Flux measurements

2.1.1 NH_3 detection with QCL

A Quantum Cascade Tunable Infrared Laser Differential Absorption Spectrometer (QC-TILDAS, Aerodyne Research Inc., USA) was used to measure NH_3 mixing ratio at 10 Hz sampling frequency for eddy covariance flux measurements. The QC-TILDAS (referred to as QCL hereafter) retrieves the NH_3 absorption spectrum at 967.3 cm^{-1} using a thermoelectrically cooled continuous wave quantum cascade laser (Alpes Lasers, Switzerland), which is scanned across the full NH_3 transition within the spectral window. A continuous wave laser has an increased power output over a pulsed laser, which was used in the version of the QCL described in detail by Ellis et al. (2010), and is therefore more suitable for measurements of high precision needed for the eddy covariance method. As illustrated in Fig. 1, the laser beam is directed into an astigmatic Herriot multiple pass absorption cell (0.5 L, 76 m effective pass length) coated with a hydrophobic coating to reduce the interaction of NH_3 with cell walls. To minimize linewidth broadening of the absorption peak, the pressure in the absorption cell is kept at approximately 4.67 kPa. A reference cell containing ethylene (C_2H_4), a less surface reactive gas that contains an absorption line near that of NH_3, is used for absorption-line lock. The signal and reference paths are focused on the same thermoelectrically cooled Mercury Cadmium Telluride (HgCdTe) infrared detector (Vigo Systems, Poland).

The laser control, spectral retrieval and mixing ratio calculations are managed by the software package TDLWintel (Aerodyne Research Inc., USA) described in Nelson et al. (2004). The measured NH_3 spectrum is fit at the 10 Hz sample frequency by convolving the laser line shape with a calculated absorption line shape based on the HITRAN (high-resolution transmission) molecular absorption database and the measured pressure, temperature and path length of the optical cell (Herndon et al., 2007). The software allows for automatic user-defined additions of zero air through the use of a solenoid valve.

Variations in pressure, temperature and other disturbances may significantly impact the instrument performance by influencing the absorption spectrum fringe pattern. Fringes are structures in the absorption spectrum which are caused by optical interferences within the laser beam path and can be responsible for signal drift if their pattern changes over time. Especially for species that are typically present in the atmosphere in the lower ppbv or pptv mixing ratio range, such as NH_3, the impact of fringes to the absorption peak range can be significant. For that reason, the operation of the QCL requires a stable environment to house the QCL and frequent background measurements with zero air to account for potential drifts in the background spectrum.

2.1.2 Setup and operation of NH_3 flux measurements

Eddy covariance flux measurements of NH_3 were performed from 28 May to 23 October 2017 on an agricultural corn field, equipped with twin flux towers near Ottawa in Eastern Canada (see Fig. 7, Pattey et al., 2006). The experimental site is located on the premises of the Canadian Food Inspection Agency (CFIA) and managed by Agriculture and Agri-Food Canada (AAFC). Prior to the measurements, the agricultural field was tilled and fertilized on 25 May using granular urea fertilizer (155 kg N ha^{-1}). The corn crop was seeded on 28 May. The QCL was installed on the west eddy covariance flux tower, which had a fetch of 200 to 500 m depending on the wind direction.

To measure the 3D wind vector for the covariance calculation, a CSAT-3 (Campbell Scientific Inc, USA) sonic anemometer was installed on the tower at 2.5 m above ground level (a.g.l.). To accommodate the growing corn canopy, the tower was raised to a measurement height of 4.5 m a.g.l. on 6 July. Water vapour (H_2O) and carbon dioxide (CO_2) were measured using a closed-path infrared gas analyser (LI-7000, LI-COR, USA). The AAFC in-house data acquisition and control system, called “REAsampl” (Pattey et al., 1996), was used to record at 20 Hz the analogue channels of the various instruments. The

REAsampl software adjusts the predetermined lags between the various close-path analysers and the vertical wind velocity, and rotate the horizontally symmetrical sonic anemometer head in the mean horizontal wind direction every hour when the hourly mean horizontal wind velocity is greater than 1.5 m s^{-1}. During the few seconds of the rotation for aligning the anemometer, the raw data are not recorded. By aligning the anemometer, flow distortion and lateral loss of covariance are minimized.

As shown in Fig. 1 the setup of the QCL consisted of five major parts: (1) the inlet system, (2) the QCL and chiller unit, (3) the valve and heating control box as well as enclosure housing (4) the vacuum pump and (5) the zero air source. The inlet was mounted at mid-vertical distance of the sonic anemometer open-path and 25 cm behind the anemometer open-path to minimize flow distortion on the wind velocity measurements by the inlet and lateral loss of covariance. The QCL uses a 10 cm quartz inlet which acts as virtual impactor to remove particulate matter from the sample air. As described in more detail in Ellis et al. (2010), about 90 % of the sample air makes a sharp turn (Fig. 1) and is pulled through the absorption cell, while 10 % of the flow, including particles larger than 300 nm due to their higher inertia, is pulled directly to the vacuum pump (TriScroll 600, Agilent, USA). To limit the condensation of water and the interaction of NH_3 with inlet surfaces, the glass inlet is internally coated with a hydrophobic fluorinated silane coating and was heated constantly to 40 °C. The glass inlet acts as a critical orifice which regulates the volume flow at the inlet. From 28 May to 27 July a glass inlet with a flow rate of 15.4 L min^{-1} and after that period a glass inlet with a flow rate of 13.4 L min^{-1}, which had a newly applied silane coating, was used. For closed-path eddy covariance measurements, a high volume flow rate is essential to keep a plug flow in the inlet system, in order to minimize HFA in the inlet system. Depending on the flow rate and the actual sample gas temperature, the Reynolds number ranged between 3000 and 3700, indicating mainly transitional flow conditions with turbulent flow in the centre and laminar flow near the tubing walls. The glass inlet was connected to the QCL via a 5.5 m long 3/8” PFA sample tube, which was insulated and controlled to 40 °C. While raising the tower on 6 July, the QCL was also raised by 2 m using wood pallets to keep a constant 5.5 m sample tube length.

The QCL, located at the bottom of the flux tower, was housed in an insulated aluminium enclosure that was equipped with two Peltier coolers to precisely control the internal temperature of the box to 28 (± 0.2) °C. Next to the QCL, the enclosure also housed the chiller (Oasis Three, Solid State Cooling Systems, USA) that is required for stable temperature control of the infrared laser and the optical and electronic parts of the QCL. To prevent the build-up of heat inside the enclosure, the intake and outtake vents of the chiller were connected to the outside of the enclosure. A dehumidifier was built in to prevent condensation inside the box.

The time series of the 10 Hz NH_3 mixing ratios and analyser parameters were digitally recorded on the QCL computer. For precise time synchronization between the post-processed digital NH_3 mixing ratios and the vertical wind velocity, an analogue signal of the NH_3 mixing ratio was recorded through REAsampl. A remote monitor was placed in a nearby trailer for regular checks and other operations like data transfer and manual valve switching, to avoid opening the temperature-controlled enclosure. Data were collected from the QCL computer regularly (every 2-4 days) and plotted for routine quality checks. To ensure optimal operation of the instrument of the QCL over the 5 month measurement period, the status of the QCL was checked regularly through remote access using a mobile hotspot.

~~The QCL glass inlet includes a port for the introduction of z~~Zero air for frequent background measurements was introduced at the front of the QCL glass inlet, designed so that ~~these flows~~zero air encounters the inlet in the same way as ambient air (Fig. 1). For zero air, a heating catalyst (Aadco Instruments, USA) was used, which scrubs NH_3 from ambient air by catalytic thermal conversion at 300 °C using palladium beads. The automatic background schedule was set to flush the inlet with zero air for 5 min at the end of every 30 min period from 28 May to 16 July. Due to an operation failure of the heating catalyst, on 17 July the zero air source was replaced by ultra high purity (UHP) compressed zero air (Praxair Canada Inc., Canada). To minimize the UHP compressed air consumption, the automated background interval was set to 1 hour with a reduced duration of 3 min from 17 July to 27 July. From 28 July to 31 August, the interval was set to 3 hours without significantly compromising on the data quality. In the final phase of measurement period, from 15 September to 23 October the background interval was set to 2 hours. While the heating catalyst was running continuously, ~~T~~the zero air gas flow was introduced into the inlet by triggering a solenoid valve installed in the valve and heating control box.

To test the effect of surface aging on the time response and to reduce the interaction of NH_3 with surfaces, regular cleaning of the glass inlet, inlet line and the absorption cell was performed using a procedure of rinsing with deionized water and ethanol, while the tubing was heated to about 80 °C during the cleaning process. The cleaning of the glass inlet was performed on 22 June, 27 July and 12 September. The inlet tubing was cleaned on 27 June, 27 July and 12 September. Along with cleaning of the glass inlet and the inlet tubing, the inner surface of the absorption cell was cleaned on 12 September.

2.2 Eddy covariance flux calculation

The processing of the NH_3 data leading to the final calculated NH_3 fluxes consisted of four major steps: (1) processing and quality control (QC) of the digital NH_3 mixing ratio data, (2) time synchronization between the quality-controlled digital NH_3 data and vertical wind velocity data recorded through REAsampl, (3) flux calculation and (4) flux random error calculation. The processing of QCL NH_3 data as well as all other processing was performed using the R software package (R Core Team, 2017).

The NH_3 mixing ratio time series were first scanned for periods of instrument failures and maintenance, which were removed. Spike detection and removal was conducted by using a running-mean low-pass filter. Spikes were identified best as data points that exceeded 3.5 times the standard deviation of a 21 point averaging window. To correct for a potential drift of the QCL between two automated background periods (varying from 30 min to 3 hr), the background mixing ratios were linearly interpolated between two consecutive background measurements and subtracted from the NH_3 mixing ratios. Following analogue acquisition using REAsampl, the 20-Hz CSAT-3 sonic anemometer and uncorrected NH_3~~ammonia~~ data were extracted from the REAsampl raw data binary files, in which the data associated with tower rotation were already removed.

The time synchronization between the NH_3 mixing ratios and vertical wind speed, which is essential for the eddy covariance flux calculation, was performed in two steps: (1) Time synchronization between the digital NH_3 data and the REAsampl data and (2) the time synchronization between the digital NH_3 data and the vertical wind velocity. For the former, a circular cross-correlation was performed between the digital and analogue NH_3 signals. Accounting for the analogue output delay, the time lag between both systems was then determined as the position of the maximum correlation. In the second step, a circular cross-correlation (using a ±5 s window) between the time synchronized sonic anemometer data and the digital NH_3 data was used to account for delays caused by the inlet system and the horizontal displacement of the CSAT-3 and the glass inlet. As the cross-correlation method between the vertical wind velocity and a scalar only works well when turbulent fluxes are large enough, a quality assessment was performed on the results of the cross-correlation. Only lag times which were less than ±2.5 s and had a cross-correlation value greater than 0.05 were used. Missing lag times were then replaced by the last previous valid lag time. To detect further outliers, lag times that were offset by more than ±1.5 s were set to the preceding lag time if the difference between the preceding and successive lag time was less than 0.5 s, indicating a spike and not a real shift in the lag time. After applying the described quality control, the standard deviation of the lag time was 1.1 s, which can be attributed partly to changes in the wind speed influencing the lag time between the sonic anemometer and inlet position.

Background on the final eddy covariance flux calculation and the required correction methods is well-documented in literature (Aubinet et al., 2012; Pattey et al., 2006). In brief, NH_3 fluxes are calculated by the covariance of the NH_3 mixing ratio (χ_{NH_3}) and the vertical wind velocity (w) multiplied by the molar density of air (ρ_m) as:

$$F_{NH_3} = \rho_m \cdot \overline{w' \chi_{NH_3}{}'} , \tag{1}$$

where $\chi_{NH_3}{}'$ and w' denote the fluctuations of NH_3 mixing ratio and the vertical wind velocity from their 30 min mean value, respectively. The NH_3 fluxes presented in this study are given in ng-NH_3 m^{-2} s^{-1}. Prior to the eddy covariance flux calculation, the 3D wind vector coordinate is typically rotated to ensure zero vertical wind velocity over the averaging period (Finnigan et al., 2003; Wilczak et al., 2001). Due to the tower rotation mechanism used in this study, the wind vector was already rotated into the mean wind direction. Variations in the air density caused by temperature and air moisture fluctuations may impact the eddy covariance flux and are typically corrected for by the WPL correction (Webb et al., 1980). The sensible heat flux induced fluctuations of ambient air temperature are expected to be efficiently damped by the heat exchange in the inlet system and the 5 m long heated inlet line. An effect of air moisture fluctuations caused by the latent heat flux on the NH_3 flux is possible, however, it was found that the effect on NH_3 fluxes is negligible (≤ 1 %) due to the relatively low concentrations of NH_3 in ambient air (Ferrara et al., 2016; Pattey et al., 1992). For these reasons, the WPL correction was not applied for the NH_3 fluxes in this study. High frequency loss corrections, like for the flux loss due to the distance between the CSAT-3 and the QCL glass inlet (Moore, 1986), were not applied to the initially calculated NH_3 fluxes as they were incorporated as part of the high frequency loss analysis discussed later in this paper.

The TK3 software package (Mauder & Foken, 2011) was used to calculate fluxes of momentum, sensible heat and latent heat and NH_3 flux quality parameters. The quality flag scheme of Foken & Wichura (1996) was used to filter for periods of low stationarity and low developed turbulence. Furthermore, the TK3 program derives the random flux errors of the NH_3 flux. The random errors include (1) the errors due to stochastic nature of turbulence and (2) the random errors due to instrumental noise (Mauder et al., 2013). The former is calculated in TK3 after the method of Finkelstein & Sims (2001), which calculates the variance of the covariance function as a combination of the auto-covariance and cross-covariance terms with changing the lag time. The random flux error due to instrumental noise is calculated in TK3 by extrapolating the auto-correlation function of the NH_3 time series towards a zero lag time (Mauder et al., 2013). As the random error calculation in TK3 was not successful for all 30 min periods, we additionally determined the instrumental noise error (σ_{cov}^{noise}) by using the variance of the zero air source measurements (conducted every 30 min to 3 hr throughout the experiment) as the variance of the NH_3 mixing ratio and by implementing that in the instrumental noise function used in Mauder et al. (2013). To be comparable to other NH_3 flux studies, we applied in addition the approach used by Sintermann et al. (2011), where the random flux error is determined for each 30 min period by the standard deviation of the covariance function (σ_{cov}^{stoch}) when using a time lag ranging between -120 and -70 s and +70 and +120 s. Using this approach, we defined the flux detection limit as $2 \cdot \sigma_{cov}^{stoch}$.

2.3 Time response determination of NH_3 measurements

A fast time response of the NH_3 measuring system is essential for performing eddy covariance measurements. To understand the processes that impact the adsorption and desorption of NH_3 to the measurement system, the knowledge of the system's NH_3 time response is important. The time response of the QCL NH_3 measurements is determined mainly by two processes (Whitehead et al., 2008): (1) the exchange of the sample air volume in the inlet line and the sample cell and (2) the adsorption and desorption of NH_3 at the inlet and sample cell walls. As a result, the time response can be described by a double exponential function giving two time constants, τ_1 and τ_2, representing the time response towards the exchange of the sample air volume and wall interactions, respectively:

$$f(t) = y_0 + A_1 \cdot exp\left(\frac{-(t-t_0)}{\tau_1}\right) + A_2 \cdot exp\left(\frac{-(t-t_0)}{\tau_2}\right), \qquad (2)$$

where t_0 is the start time and y_0 the offset from zero (Fig. 2); A_1 and A_2 are proportionality coefficients which account for the contribution of each process to the overall time response. Accordingly, the percentage contribution of the wall interaction processes can be described as (Ellis et al., 2010):

$$D = \left(\frac{A_2}{A_1 + A_2}\right) \cdot 100\ \% \, . \qquad (3)$$

Together with the time constants τ_1 and τ_2, D can be used to evaluate the performance of the QCL system with respect to its time response. To determine the time response for our instrument setup, the double exponential function (Eq. 2) was fitted to the step change in NH_3 mixing ratios when switching from ambient air to zero air measurements as part of the automated background correction. Those fits were performed for each background period in order to obtain the temporal variation of the time response over the course of the entire measurement period.

2.4 Analysis of flux loss due to high frequency attenuation

2.4.1 Ogive method

The attenuation of the high frequency scalar time series due to a slow response leads to an underestimation of the calculated eddy covariance flux. Both theoretical and experimental approaches are used to quantify the flux loss and ultimately correct for it; a summary is given in Foken et al. (2012). For NH_3 the HFA needs to be determined experimentally, since to date no adequate description of the surface adsorption and desorption processes exists. Experimental approaches typically compare the co-spectrum of the vertical wind velocity and the attenuated scalar time series to the co-spectrum of a non-attenuated reference flux. As a reference flux the sensible heat flux is most often used, either from direct measurements or from parameterization available in literature (Kaimal and Finnigan, 1994). In this study we used the ogive method described in Ammann et al. (2006). The ogive of a scalar flux (Og_{ws}) is calculated by the cumulative integral of the co-spectrum (Co_{ws}) as

$$Og_{ws}(f) = \int_{1/t}^{\infty} Co_{ws}(f)\, df \qquad (4)$$

over the observed frequency range, beginning with the lowest frequency ($1/t$, where t is the averaging interval). If the ogive is normalized by the covariance, the ogive value at the highest frequency is 1. The flux loss is derived by scaling the normalized ogive of the scalar flux to the normalized ogive of the sensible heat flux at a given limit frequency (f_0). The scalar ogive value at the highest frequency represents then the flux attenuation factor (between 0 and 1). The limit frequency is defined as the highest frequency at which no HFA occurs and can be determined from the comparing the scalar co-spectrum to the sensible heat flux co-spectrum.

Ideally, a reference scalar is used which shows the highest scalar similarity to the investigated flux. The water vapour flux is expected to have a similar sink and source distribution than NH_3, but the measured flux may experience high-frequency loss if measured with a closed-path analyser. Therefore, we used in this study the measured non-attenuated sensible heat flux as a reference.

2.4.2 Time response ~~transfer function~~ method

Another approach to correct for the HFA is to simulate the flux loss by knowing the flux loss transfer function~~.~~, which represents the flux attenuation factor as a function of frequency. ~~The transfer function can be indirectly determined through the system's time response, which was determined over the entire measurement period as described in Sect. 2.3.~~The transfer function can be obtained by ~~The method~~ applying~~ies~~ a low-pass filter, which represents the HFA of the system, to the time series or flux of a non-attenuated scalar ~~time series~~ and then ~~compares~~ comparing the filtered and non-filtered ~~co-spectra~~fluxes. In this study, we determined t~~T~~he transfer function~~ can be indirectly determined~~ through the system's time response, which was determined over the entire measurement period as described in Sect. 2.3. As for the ogive method, we used the sensible heat flux as a reference flux.

A low pass-filter can be applied either (1) in the frequency domain or in the (2) in the time domain. For the former method, a transfer function is applied to the sensible heat flux co-spectrum, which we modified using both τ_1 and τ_1 from Eq. 2. However, the low-pass filter effect of the inlet tubing introduces next to the attenuation of high frequency amplitudes a phase shift (Horst, 1997; Massman and Ibrom, 2008). For that reason we applied a low-pass filter in the time domain to the high frequency temperature time series. This method accounts for the phase shift and was used in the past to simulate the HFA effect of eddy covariance water vapour fluxes (Ibrom et al., 2007) and of relaxed eddy accumulation systems (Moravek et al., 2013). In the time domain, a low-pass filtered scalar time series (c_{att}) is retrieved as

$$c_{att_n} = c_n \cdot A + (1 - A) \cdot c_{att_n}, \qquad (5)$$

where c is the non-attenuated scalar time series and A is the filter constant. For a given sampling frequency (f_s), this constant depends on the cut-off frequency (f_c), which is the frequency at which the filter reduces by a power of two:

$$A = 1 - e^{-2\pi\cdot(f_c/f_s)}, \qquad (6)$$

where f_c can be characterized by the time constant τ:

$$f_c = \frac{1}{2\cdot\pi\cdot\tau}. \qquad (7)$$

Since the time response for NH_3 is described by two time constants, we low-pass filtered the high frequency temperature time series using both τ_1 and τ_2, where τ_1 is the time constant describing the exchange of sample air volume and τ_2 is the time constant accounting for wall interactions. The respective low-pass filtered time series, c_{att_1} and c_{att_2}, can be then combined as

$$c_{att} = (1 - D/100) \cdot c_{att_1} + D/100 \cdot c_{att_2}, \qquad (8)$$

using the D value from the time response analysis. The transfer function using the time domain low-pass filter method ($T_{time}(f)$) is then defined as the ratio between the attenuated and non-attenuation sensible heat flux co-spectrum

$$T_{time}(f) = \frac{Co_{wc_{att}}(f)df}{Co_{wc}(f)df}. \qquad (9)$$

To account to for the time lag introduced by the phase shift of the low-pass filter, a circular cross-correlation between the overall low-pass filtered temperature and the vertical wind velocity time series was performed before. The flux attenuation factor using the time response method (α_{tr}) is then be determined by the ratio of the filtered co-spectrum and the non-filtered co-spectrum of the sensible heat flux, which is equal to the ratio of the attenuated and non-attenuated sensible heat flux covariance:

$$\alpha_{tr} = \frac{\int_o^\infty Co_{wT_{att}}(f)df}{\int_o^\infty Co_{wT}(f)df} = \frac{cov\langle w, c_{att}\rangle}{cov\langle w, c\rangle}. \qquad (10)$$

To investigate the possible NH_3 flux loss over the measurement period, the flux loss was simulated for all 30 min periods, using τ_1, τ_2 and D values that represent the range of observed time responses.

3 Results

3.1 Measured NH_3 fluxes, random flux error and flux detection limit (before HFA correction)

The QCL eddy covariance measuring system was operated over a period of 149 days between May and October 2017, covering a total of 7132 flux measurement periods. Times of system maintenance, quality control checks, and other system downtimes were discarded from the dataset, resulting in a flux data coverage of around 85 % (Table 1).

Figure 3 shows the ~~flux~~ statistics of flux magnitudes for each month from May to October before applying any HFA correction.~~,~~ Flux magnitudes are compared to the median diurnal flux detection limits of each month. As illustrated in the top right corner of each month, ~~with distinct periods of~~the diurnal flux magnitudes were comprised of both NH_3 emission and deposition fluxes. Although fluxes in May only represent four days, the overall maximum flux of around 500 ng m^{-2} s^{-1} was observed in that period. While June and July were mainly dominated by small fluxes, typically less than ±10 ng m^{-2} s^{-1}, in August clear emission was observed with a daytime median value around 20 ng m^{-2} s^{-1}. September marked an emission to deposition transition period, with significant deposition fluxes reaching to -300 ng m^{-2} s^{-1}. In October, fluxes were dominated by deposition, with a median daytime value around -30 ng m^{-2} s^{-1}. Over the entire period, the daytime median flux was 8.6 ng m^{-2} s^{-1} during periods of emission and -19.87 ng m^{-2} s^{-1} during periods of deposition (Table 1). Night time fluxes were significantly lower, with median values of 3.5 and -4.27 ng m^{-2} s^{-1}, respectively, showing clear diurnal cycles during periods of high emission and deposition.

The flux statistics are affected by the choice of the flux quality flags used to remove periods of weakly developed turbulence or non-stationarity (Foken and Wichura, 1996). A quality flag ≤ 3 is typically used for fundamental research, whereas fluxes with quality flag ≤ 6 are used for long-term flux data sets. We only used fluxes with a quality flag ≤ 3, leaving 68 % of daytime and 46 % of night time fluxes (Table 1).

The random flux error due to instrumental noise (σ_{cov}^{noise}) is dependent on the precision of the QCL and variations in the friction velocity (u_*). Over the course of the field campaign, an average precision of 0.085 (±0.010) ppbv at the 10 Hz sample frequency was achieved, which was independent of the measured NH_3 mixing ratio. The resulting median flux error was 0.17 ng m^{-2} s^{-1} for daytime and 0.08 ng m^{-2} s^{-1} for night time fluxes; much lower than the median observed fluxes (Table 1). In contrast, the random error derived from the lag time shift (σ_{cov}^{stoch}) was significantly larger, with median values of 1.61 ng m^{-2} s^{-1} during daytime and 0.72 ng m^{-2} s^{-1} during night time. However, still only 11.6 % of the total flux data were below the detection limit (2.15 ng m^{-2} s^{-1}), which shows the overall good performance of the QCL eddy covariance measuring system.

3.2 High frequency attenuation

3.2.1 Ogive method

We applied the ogive method to the co-spectra of sensible heat and NH_3 flux. Figure 4 shows an example of the normalized co-spectra. To illustrate the effect of HFA, the co-spectra are multiplied by the frequency; HFA is indicated if the slope of the NH_3 co-spectrum in the inertial subrange (high frequency part of spectrum) is steeper than the slope of the sensible heat flux co-spectrum. While this is not clearly visible in the co-spectra (by comparing against the expected -4/3 slope line in the inertial subrange), the ogives show a clear underestimation of the NH_3 flux at higher frequencies, illustrated by the flattened NH_3 ogive curve at high frequencies. Applying the ogive method to all 30-min periods yields a frequency distribution of the attenuation factor (Fig. 5). As the ogives may show significant noise or fluctuations, the choice of the limit frequency for the determination of the scaling factor is critical. For that reason three limit frequencies of 0.05 Hz, 0.067 and 0.10 Hz were chosen representing time scales of 20, 15 and 10 s, respectively. Only periods were used where the standard deviation of the scaling factors determined at those three limit frequencies was smaller than 5 %. Furthermore, only data periods were used where both the NH_3 and sensible heat flux were significant and of sufficient data quality (TK3 flag ≤ 3). After applying that filter, the median flux attenuation factor was calculated to be 0.83, corresponding to a flux loss of 17 %. The spread of the observed factors was significant with 50 % of the values lying between 0.75 and 0.91; the standard deviation was 16 %. Also, for some periods the attenuation factor was above one, which is most likely caused by uncertainties in the ogive method.

To give insights into the causes of the NH_3 flux loss, the attenuation factor was analysed for dependencies on different parameters. No clear change of attenuation factor was observed over time, which would have suggested an effect of surface aging or cleaning. Due to the uncertainties in the ogive method, the noise in the attenuation factors was larger than the effect of surface aging or cleaning. Also, no correlation of the attenuation factor with ambient air humidity was found. The highest variation of attenuation factors occurred at conditions of neutral atmospheric stability, an indication of the limitations of the ogive method during these conditions. However, a slight decrease of the attenuation factor with increasing horizontal wind speed (u) was found (Fig. 6 and Fig. S1), which is expected due to the shift of the turbulence spectra to higher frequencies with increasing wind speed. Given the non-Gaussian distribution of attenuation factors at some wind speeds, we used a quantile linear regression to~~The linear regression yields~~ obtain a function of the flux attenuation factor using the ogive method (α_{ogive}) with u (in m s^{-1})~~ as~~:

$$\alpha_{ogive} = f(u) = -0.031\cancel{28} \cdot u + 0.9\cancel{7}4\ . \tag{$\cancel{9}11$}$$

~~However, with an~~Since the majority of used data is clustered between wind speeds of 0.5 and 2.5 m s^{-1}, the correlation with wind speed is only weak as illustrated by a R^2 value of 0.04~~, the correlation~~ of the least squares linear regression~~ is very weak~~. The correlation might be impacted by changes of the aerodynamic measurement height, due to tower raise and the growth of the corn canopy over the season.~~-~~ However, as no clear correlation of the attenuation factor with time was found, this effect is not accounted for in the presented relation with horizontal wind speed.

3.2.2 Time response

The double exponential function used to determine the system's time response is characterized by τ_1, τ_2 and the D value. The median value for τ_1 was 0.6 s. That value is slightly higher than the calculated time constant for the exchange of air volume in the 0.5 L absorption cell (~ 0.1 s). The time response needed to exchange the air volume in the inlet tubing is significantly less (< 0.03 s), due to its small volume and low pressure (< 15 kPa) in the inlet tubing. The time constant τ_2, representing the time scale for NH_3 surface interactions, showed a median value of 27 s. Both τ_1 and τ_2 did not exhibit a clear trend over time, nor a correlation with humidity or other parameters. In contrast, the D value revealed distinct differences over time. Figure 7 shows the evolution of the D value over the course of the field campaign together with times of inlet, tube and cell cleaning. Initially, D values were around 20 % and then increased steadily to more than 50 % at the end of June. While cleaning of the glass inlet and the inlet tube in June did not directly lead to a decrease in the D value, the cleaning of the glass inlet and inlet tubing on 27 July led to a visible decrease of the D value. On September 12, when the inlet, tubing and the surface of the absorption cell was cleaned, the largest decrease of the D values after cleaning down to 10 % was observed. Additionally, a significant overall decrease of D values was observed following July 17, after switching the zero air source from the heating catalyst to the UHP compressed air. Since the heating catalyst scrubs NH_3 from ambient air, the moisture level of the heating catalyst zero air is more similar to ambient air than that of the dry UHP compressed air. The D value differences for the two zero air sources might be therefore caused by different moisture levels. However, no distinct correlation of the D value with ambient air humidity was found for the heating catalyst period. A decrease of D values with increasing ambient air NH_3 mixing ratios, as discussed in Ellis et al. (2010), was detected (Fig. 8), suggesting a larger relative importance of adsorption and desorption processes at lower NH_3 mixing ratios. The increase of D values at lower NH_3 mixing ratios may be also due to the variation of D values caused by a larger uncertainty of the double exponential fit with small mixing ratio changes. While the relative random errors of A_1 and A_2 from double exponential fit increase exponentially with decreasing NH_3 mixing ratios, the propagated random error of D was typically below 10 % for NH_3 mixing ratios above 0.5 ppbv. For lower mixing ratios only D values with a relative error of less than 50 % were used.

3.2.3 Time response ~~transfer function~~ method

To investigate the effect of the measured time response on the NH_3 fluxes, the flux loss was simulated using the time response ~~transfer function~~ method. As the ~~observed~~ time constants τ_1 and τ_2 ~~were fairly constant~~did not show distinct trends over time like the D value, ~~τ_1 and τ_2~~ they were fixed at 0.6 and 27 s, respectively. The flux loss was simulated for D values of 0, 20, 40 and 60 %, which represents the observed range of D. Figure 9 shows $T_{time}(f)$ ~~the calculated transfer functions~~ for the four scenarios and their effect on the ogives of sensible heat flux for a selected 30 min period. To illustrate the contributions of the two time constants τ_1 and τ_2 as well as the influence of the phase shift, the respective frequency domain transfer functions $T_{f_1}(f)$ and $T_{f_2}(f)$ are shown. Since the frequency domain transfer functions used here only account for the attenuation of the signal amplitudes and not the phase shift, their sum ($T_f(f)$) underestimates the flux loss compared to the time domain low-pass filter approach used in this study. ~~As the results illustrate~~For the 30 min period shown here, the flux loss ranged~~s~~ from 21~~0~~ to 64~~47~~ %, increasing with higher D values, representing a higher contribution from the slow time constant that reflects adsorption/desorption. Applying the simulation for flux data from the entire measurement period, a clear decrease of the flux attenuation factor with increasing horizontal wind speed was observed (Fig. 10), which is explained by a shift of the co-spectrum to higher frequencies with increasing wind speeds. The linear regression lines for each simulation scenario are displayed in Fig. 10 including the respective linear regression functions. By expressing the slope (m) and the intercept (c) as a function of D through linear regression ($f_{m,c}(D) = m_{m,c} \cdot D + c_{m,c}$), we can describe the flux attenuation factor using the time response method (α_{tr}) as a single function of u and the D value as:

$$\alpha_{tr} = f(u,D) = (m_m \cdot D/100 + c_m) \cdot u + m_c \cdot D/100 + c_c \ .$$
(~~10~~12)

For the presented dataset, the linear regression yielded m_m = 0.~~018~~036, c_m = -0.~~041~~047, m_c = -0.~~49,~~83 and c_c = 0.93. The overlap of the regression lines of this generalized function with all individual regression lines in Fig. 10 shows the strong linear correlation of the flux attenuation factor with both u and the D value. In the case of D = 0, Eq. 12 represents the damping that is not due to the wall interactions and would also be applicable to other, non-sticky, trace gases. After deriving α_{tr} t~~T~~he NH_3 fluxes are then corrected individually for every 30 min period by dividing by α_{tr}.

4 Discussion

4.1 Random flux error and flux detection limit

Closely connected to the issue of HFA is the requirement of the NH_3 measurement system to resolve small NH_3 mixing ratio fluctuations at high time resolution. Due to the challenges in measuring small NH_3 fluxes, the quantification of the random flux error and flux detection limit is essential for the quality assessment and interpretation of NH_3 fluxes. Distinguishing between two types of random errors, we found that the error due to instrumental noise (σ_{cov}^{noise}) was significantly lower than the stochastic random error (σ_{cov}^{stoch}). This can be attributed to the high precision of the QCL measurement achieved during the measurement period, resulting in median σ_{cov}^{noise} of 0.13 ng m^{-2} s^{-1}. To our knowledge, continuous wave QCL spectrometers are currently the most precise commercially available NH_3 measurement systems. Since the instrumental noise affects also σ_{cov}^{stoch}, σ_{cov}^{stoch} (median 1.08 ng m^{-2} s^{-1}) can be used as the total random flux error. Investigating the entire measurement period, we found increasing σ_{cov}^{stoch} values with a higher (absolute) flux magnitude, although, due to variations, no clear relationship could be formulated. Still, for (absolute) flux magnitudes above 20 ng m^{-2} s^{-1}, the median random flux error was 13 %, giving a general random error estimate for those higher observed flux magnitudes.

Defining the flux detection limit as 2·σ_{cov}^{stoch}, the median value was 2.15 ng m^{-2} s^{-1}, which is about half of what was reported by Sintermann et al. (2011) for flux measurements using PTR-MS after slurry application (4.5 ng m^{-2} s^{-1}) and 4.4 times lower than the detection limit given by Zöll et al. (2016) for measurement above a peatland (9.4 ng m^{-2} s^{-1}), using the same QCL analyser used in this study. While our analysis of σ_{cov}^{stoch} covered the entire measurement period, Sintermann et al. (2011) determined their flux detection limit during a period when no significant NH_3 fluxes were detected, most likely leading to a smaller flux detection limit calculation than with our approach. Since we observed that σ_{cov}^{stoch} can vary significantly over time, when filtering the NH_3 flux data the respective flux detection limit value of the relevant flux period seems to better reflect different turbulence conditions.

4.2 Parameters affecting time response

The QCL's time response for NH_3 was determined over the 5 month measurement period, providing a large dataset of different operational and environmental conditions which may impact the time response. Known parameters affecting the NH_3 time response are properties of the ambient air like humidity and magnitude of NH_3 mixing ratios, surface material and surface-adsorbing matter, surface temperature and sample flow conditions. Since the temperature of the inlet and the sample flow rate were not significantly changed during the field campaign, we did not investigate the influence of surface temperature and sample flow conditions on time response. From the findings of our study, we discuss and summarize in the following the impact of humidity, ambient NH_3 mixing ratios, surface contamination on time response, together with investigations on the availability of surface adsorption sites.

4.2.1 Ambient air humidity

Since we determined the time response from the decay of NH_3 mixing ratios after switching from ambient to zero air, the humidity of the zero air source is important. While the UHP compressed air was dry, the humidity of the heating catalyst zero air is closer to ambient air humidity. There was a clear improvement in the time response when using the dry UHP compressed air. This indicates that humidity has an effect on the time response if dry air is compared with ambient air of average humidity. However, no correlation was found between time responses and ambient air humidity when the heating catalyst was used as zero air source. Since the amount of water vapour in the measured ambient air was about 10^6 times higher than the amount of NH_3, a humidity effect on the NH_3 time response might be not noticeable at ambient humidity levels. Since there are only limited adsorption sites for water molecules available on the inlet and cell surfaces, low humidity levels may already lead to a saturation of surface sites. Once all surface sites are occupied by water molecules, the time response is insensitive to variations in ambient air humidity, which might explain why no correlation of the time response with ambient air humidity was observed. Ellis et al. (2010) found the time response to degrade with the relative ambient air humidity, however, their data was collected under significantly higher NH_3 mixing ratios reaching up to 1000 ppbv and the correlation was much weaker when the inlet line was heated to 40 °C.

4.2.2 Ambient air NH_3 mixing ratio

As shown in Fig. 8, the relative importance of the slow component of the system's time response was higher with lower NH_3 mixing ratios. While our ambient air measurements were mainly below 10 ppbv, the laboratory study by Ellis et al. (2010) saw the same effect for NH_3 mixing ratios between 30 and 1000 ppbv. The proposed hypothesis for this effect is that at lower NH_3 mixing ratios a larger proportion of the ambient NH_3 can interact with surface adsorption sites, which leads to a larger D value. As the time response experiments were performed by switching from an ambient mixing ratio to zero air, the time response could be improved if the start and end NH_3 mixing ratio are offset by a fixed NH_3 mixing ratio, leading to higher passivation of the surface material. However, in a laboratory test (not shown), we found that the time response was not significantly improved when switching between two higher mixing ratios of the same mixing ratio difference. This may imply that the time response is also governed by the magnitude of the NH_3 change instead of the NH_3 mixing ratio alone. While for the former the NH_3 high frequency loss would be related to the NH_3 flux magnitude, for the latter it would be dependent on the NH_3 mixing ratio, which has implications for the flux loss correction. For our dataset a mixing ratio decrease of about 10 ppbv increased the *D* value by about 10 % (Fig 8.), which would result in an additional flux of about 10 % (Fig. 10), However, since more tests are needed to distinguish whether the NH_3 flux magnitude or NH_3 mixing ratio are the determining factor, the correction factors developed here do not included this additional correction.

4.2.3 Inlet system surface material and contamination

Previous studies have shown the impact of surface material on time response, with PFA or PTFE being the most suitable material for inlet tubing (Whitehead et al., 2008; Zhu et al., 2012). Surface aging and contamination are known to be important factors, thought it has been not satisfactorily quantified in the past. The presented 5 month dataset shows how the time response gets slower with time, most clearly visible in the increasing *D* values in the first month of the measurements (Fig. 7). The fact that the time response is not improved after every cleaning of the inlet parts and absorption cell shows the complexity of NH_3 time response and the importance of the other factors affecting it.

4.2.4 Availability of surface sites and active passivation

The discussion of parameters controlling time response shows that the mechanisms that govern the time response of NH_3 measurements are still not well understood. One reason for this is the lack of knowledge on the amount of available surface sites for adsorption of NH_3 under the different conditions. Also, the amount of NH_3 adsorbed to the surface is uncertain. It can be estimated by introduction of 1*H*,1*H*-perfluorooctylamine into the sample inlet (Roscioli et al., 2015), where the NH_3 originally adsorbed to the surface is replaced by the amine and measured by the QCL. By integrating the NH_3 peak from the desorption process, Roscioli et al. (2015) estimated a density of NH_3 of $8 \cdot 10^{14}$ molecules cm^{-2} on the surface of their QCL system. We performed the same experiment for our system in the laboratory after the completion of the field campaign and found a surface coverage of about $4 \cdot 10^{13}$ molecules cm^{-2}, which is about a factor of 20 lower than the value observed by Roscioli et al. (2015). As we carried out the test using the same tubing and glass inlet (both not cleaned) that were used during the campaign, the desorbed NH_3 amounts represents the amount of NH_3 at the end of the measurement campaign, although it cannot be excluded that some NH_3 was desorbed from the surface after the experiment. Repeated application of the amine after exposure of the inlet to a calibration source of NH_3 (8 ppbv) showed that the desorbed NH_3 was proportional to the NH_3 exposure time. This shows the direct link between NH_3 exposure and adsorbed surface NH_3. However, similar experiments would be needed for a wider range of conditions to obtain a quantitatively meaningful characterization of adsorbed surface NH_3 and better understanding of available NH_3 adsorption sites. Together with the NH_3 adsorption capacity of the surface, a determination of the adsorption and desorption rate constants is necessary to describe the interaction of NH_3 with the surface material and to quantify the HFA during field conditions through adsorption and desorption mechanisms.

4.3 High frequency loss correction for NH_3 fluxes

The knowledge about the parameters affecting the time response of NH_3 measurements is important to make improvements on the NH_3 measurements and to find the appropriate high frequency flux loss correction method. In past studies, both experimental and theoretical approaches have been applied for the correction of NH_3 fluxes. Although experimental approaches were used in this study, we discuss in the following also theoretical approaches, based on the findings from the presented 5 months flux dataset.

4.3.1 Theoretical approaches

In the processing of eddy covariance fluxes, theoretical approaches to correct for the HFA are commonly applied. In this approach, transfer functions, which describe the HFA, are multiplied with the reference co-spectrum. The reference co-spectrum is either derived from parameterizations or from direct measurements of a non-attenuated flux, such as the sensible heat flux. For NH_3 fluxes, the transfer function has to account for the NH_3 surface interaction, as it has been formulated for fluxes of water vapour (Ibrom et al., 2007; Massman and Ibrom, 2008). Ferrara et al. (2012, 2016) used a reference co-spectral model combined with theoretical transfer functions for the effect of lateral/longitudinal separation between the sonic anemometer and the NH_3 measurement and for the HFA along the inlet tubing and within the QCL absorption cell. The main parameters controlling these transfer functions are wind speed, inner diameter and length of tubing, sample flow rate and the absorption cell time constant. The results from our study showed that the time response of the NH_3 measurements over the 5 month period was governed by desorption and adsorption processes of NH_3 on surfaces, which are not adequately considered in these transfer functions. Although short inlet tubing, a high sample flow rate, low tube pressure conditions and heating of the inlet line are factors that minimize the time response (Ferrara et al., 2012, 2016), we found that changes in operational conditions, such as humidity and surface contamination, can have significant impacts on the time response and therefore the flux attenuation. As argued also by Sintermann et al. (2011), a more mechanistic understanding of surface processes is necessary for a theoretical transfer function that adequately describes the time response of NH_3. For that reason, approaches that evaluate the high frequency flux loss from measurements are necessary.

4.3.2 Experimental approaches

The high frequency flux loss in experimental approaches is determined by comparing the co-spectrum of the attenuated scalar flux to the co-spectrum of a non-attenuated flux. The ogive method (used for NH_3 fluxes by Ferrara et al. (2012), Sintermann et al. (2011), Zöll et al. (2016) and in this study) uses the cumulative co-spectra, and is mathematically equal to approaches that use the ratio of the scalar co-spectrum and the reference co-spectrum directly (used for NH_3 fluxes by Whitehead et al., 2008). Differences are mainly apparent in data pre-processing, averaging or fitting procedures used. Since variations of co-spectra from the ideal shape can be significant, the method which yields the most robust relation between the NH_3 and reference ogives (or co-spectra) is preferred. In this study, we used the standard deviation of the attenuation factor from three different limit frequencies, the flux magnitude and the flux quality flag to filter the dataset, yielding a median flux attenuation factor of 0.83. The flux loss was significantly less than for NH_3 fluxes reported by Zöll et al. (2016), who found for their NH_3 QCL a median flux attenuation factor of 0.67. Also using a NH_3 QCL system, Ferrara et al. (2012) determined an average correction factor of 1.37 with the ogive method, which translates to a flux attenuation factor of 0.73. Reasons for the differences in flux attenuation factors may be linked to operational differences. In contrast to our study and Zöll et al. (2016), the system by Ferrara et al. (2012) had a lower flow rate with laminar flow conditions, which would be expected to result in more significant attenuation factors. In contrast, their heated inlet line was shortest (2.5 m), followed by Zöll et al. (2016) (3 m) and our study (5.5 m). Regular cleaning of the QCL system over the 5 month period, likely contributed to the low flux attenuation in our study. Another factor affecting the flux loss is the flux magnitude. For example, the NH_3 fluxes presented by Ferrara et al. (2012) are significantly larger, covering six days directly after urea application to the agricultural field, which may explain the moderate flux attenuation despite the laminar flow conditions. Finally, differences in data processing and filtering of ogive results can be responsible for some of the discrepancies.

We observed a slight decrease of the flux attenuation factor with increasing horizontal wind speed, as was reported by Sintermann et al. (2011). However, uncertainties in the flux attenuation factor may be the reason why the correlation with wind speed was very weak ~~(R^2 = 0.04)~~. Zöll et al. (2016) did not find a correlation with wind speed, stating a random error of the flux attenuation factor of 15 %. In our study, the random error of the attenuation factor was 19 %, while the flux attenuation factor in Ferrara et al. (2012) had a variation of 27 %. Again, the data processing and data filtering method largely impact the standard variation of the ogive method results. For example, as shown in Fig. 6, our data included attenuation factors greater than 1, which are not realistic, but were included for statistical reasons. Next to the random uncertainty, Zöll et al. (2016) states that there might be potential systematic deviations of the attenuation factor, caused by HFA that is not detected by the ogive method; however, it is unclear which low-pass filtering processes might be responsible for that.

Due to the uncertainties in the ogive method and its failure to reflect the operational changes (such as inlet cleaning and tube aging) that we expected to affect the attenuation, we used the time response measurements to quantify the flux loss over the experiment period. We found that the time response ~~transfer function~~ method captured cleaning and surface aging over time. Also, from the change of the zero air source to dry UHP compressed air we found evidence that time response is sensitive to humidity, although a distinct correlation between ambient humidity and the time response could not be found. Furthermore, the applicability of the time response ~~transfer function~~ method is not limited to the flux magnitude, and therefore can also be used to determine the flux attenuation of low NH_3 fluxes where the ogive method shows larges uncertainties.

To correct the NH_3 flux loss with the time response ~~transfer function~~ method, we determined the attenuation factor as a function of wind speed and the D value from the time response measurements (Eq. ~~10~~12). Since the observed D values showed significant fluctuations, which are attributed to the random uncertainty of the double exponential fitting procedure, we calculated a moving median D value as illustrated in Fig. 7. By using the smoothed D values, changes in the time response caused by operational changes and differences in mean environmental conditions over the course of the 5 months experiment are accounted for. Since we link the significant change of the time response when switching the zero air source to the drier

UHP compressed air, this effect has to be corrected for if the time response method is applied to the entire dataset. We therefore increased those *D* values which were derived with the UHP compressed air by a fixed absolute value of 20 % (blue data points in Fig. 7), which was the approximate difference of *D* values observed at the time of switching between the two sources. Applying the corrected *D* value in Eq. ~~10~~ 12 to the entire flux dataset, the median flux attenuation factor is 0.~~67~~54, corresponding to a median flux underestimation of ~~34~~ 46 % that has to be corrected for. This is significantly larger than the median flux loss from the ogive method, which was 17 % (Fig. 5). Using the relationship of the ogive flux attenuation factor with wind speed (Eq. ~~9~~11) yields a median flux loss of only ~~8~~ 11 % for the entire dataset. However, the relation might be skewed by flux attenuation factor values above 1, which were not rejected.

After application of the HFA correction, the magnitude of the NH_3 fluxes presented in Fig. 3 and Table 1 increases by the correction factor we derived with the time response method. While it is not within the scope of this paper to discuss the underlying processes that governed the NH_3 exchange at the site, the plausibility of the NH_3 fluxes is important and linked to the flux quality control. We used the WindTrax dispersion model (Thunder Beach Scientific, Canada) to estimate the range of possible NH_3 fluxes during periods when the highest NH_3 fluxes were observed for different scenarios of background NH_3 mixing ratios (see Supplementary Material for details). The analysis shows that the HFA-corrected measured NH_3 fluxes are within the range of fluxes predicted by WindTrax. During the peak emissions, the NH_3 emissions estimated by WindTrax emission are at most 1.5 times higher than the measured fluxes. This shows that a significant underestimation of the HFA correction with the time response method is unlikely. Furthermore, we found that the corrected NH_3 fluxes are in agreement with preliminary resistance model results, which underlines the plausibility of the presented NH_3 fluxes.

We showed that the time response ~~transfer function~~ method is a technique that can be used to correct for the HFA of NH_3 fluxes. The method accounts for changes in operational and environmental conditions over time, with a significantly lower random uncertainty than the ogive method. However, the applicability is largely dependent on the correct determination of the time response. The change of *D* values after switching between zero air sources showed that it is crucial to perform time response experiments under the conditions of the flux measurements. This entails using similar air humidity conditions and NH_3 mixing ratios as in ambient air, but also NH_3 step changes of similar magnitude than the NH_3 fluctuations during the eddy covariance measurements. For example, the time response can be determined between two different NH_3 levels, as it was done by Brodeur et al. (2009), by adding NH_3 from a NH_3 source to ambient air. However, challenges to use such a system in field conditions remain, as short-term fluctuations (< 5 min) of ambient air would have to be filtered out in order to obtain a reliable estimation of the double exponential fit and therefore the time response.

5 Conclusions

Challenges in measuring atmospheric NH_3 at a fast sampling rate have limited the application of the eddy covariance technique to investigate the surface-atmosphere exchange of NH_3. While several studies have presented eddy covariance measurements, there is still a poor understanding on the drivers governing time response and how to account for HFA in the post-processing.

In the present study, we deployed a continuous-wave QCL from May to October 2017 to measure NH_3 eddy covariance fluxes above a corn field in Eastern Canada.

Over the experimental period, the eddy covariance system was operated without major interruptions, while regular maintenance of the QCL guaranteed a consistently high precision of the 10 Hz NH_3 signal (90 pptv). The median random flux errors due to the instrumental noise was insignificant (0.1 ng m^{-2} s^{-1}, 4 % using absolute NH_3 fluxes) compared to the stochastic error of the eddy covariance measurement (1.1 ng m^{-2} s^{-1}, 15 % using absolute NH_3 fluxes), which is independent from the eddy covariance system performance. The median flux detection limit before applying the HFA correction was 2.15 ng m^{-2} s^{-1}, leading to only 11.6 % of flux data below the detection limit. Considering for the HFA flus loss with the time response method the median flux detection limit was ~~3.21~~4.08 ng m^{-2} s^{-1}.

Through the 5 month measurement period, we obtained flux measurements over a large range of environmental and operational conditions, which allowed us to study the parameters affecting the instruments time response and its effect on the NH_3 flux measurements. While humidity is thought to be a factor affecting time response, we found no clear correlation between the ambient humidity and the time response. Instead we found that the time response was improved when dry UHP compressed air was used, which suggests the existence of a humidity effect. For that reason, the time response *D* value had to be corrected to account for the higher ambient humidity under flux measurement conditions. While we saw significant improvement of the analyser's time response after cleaning of the QCL sample cell, the cleaning of inlet tubing and the QCL glass inlet did not systematically lead to significant time response improvements. This shows the complexity of mechanisms governing NH_3 time response and the need for the appropriate flux loss correction method.

From the flux attenuation analysis with the ogive method, we determined a median flux loss of only 17 % (±16 %), which shows the overall good performance of the eddy covariance system. As for the time response, no correlation between the flux loss and ambient humidity was found, instead a slight increase of the flux loss with increasing horizontal wind speed, which was expected due to the shift to smaller turbulent scales at higher wind speeds. The ogive method did not detect the change of time response due to surface aging and instrument cleaning, which we attribute to noise and fluctuations in the co-spectra. Due to the uncertainties in the ogive method and complexity of NH_3 time response, we introduce the use of the time response ~~transfer function~~ method for NH_3, which simulates the flux attenuation according to measured changes in the system's time response, and thereby accounts for changes of the time response, for example due to surface aging. We provide a correction factor as a function of the time response *D* value and the horizontal wind speed. The obtained flux correction factors ranged from 1.35~~2~~ to 2.~~11~~69, with a median flux loss of ~~34~~ 46 %, which is substantially higher than the values obtained through the ogive method. We argue that due to the complexity of NH_3 adsorption and desorption processes to surfaces, it is important to determine the time response over the course of a field experiment, also to make better informed decision on instrument operation and maintenance. In the future, improvements have to be made on how the time response is determined over the course of a field experiments. Also, a more in-depth understanding of NH_3 surface adsorption and desorption processes is necessary to develop theoretical frameworks to correct the flux loss of NH_3 eddy covariance measurements and give guidance for improved fast time response NH_3 measurements.

Author contribution

AM and SS performed and quality controlled the NH_3 measurements. LP and EP obtained the turbulence and H_2O measurements and managed the experimental site. AM performed the NH_3 flux calculation and quality control and did the high frequency attenuation analysis. JGM and EP initiated the project. AM wrote the manuscript with comments from co-authors.

Acknowledgements

We acknowledge Dr. Stuart Admiral for his assistance at the experimental site. We thank Amy Hrdina and Theodora Ho-Yan Li for their help throughout the field campaign. We greatly thank the University of Toronto machine shop for their dedicated work on the temperature controlled QCL enclosure. We also thank Undine Zöll and the technicians from different companies for discussions on the enclosure design and temperature management. The study was funded by AAFC Science and Technology Branch Project J-001318 on Improve N sustainability of field crops led by Dr. Elizabeth Pattey. Partial funding support was provided by a Natural Science and Engineering Research Council Discovery Accelerator Supplement awarded to Dr. Jennifer G. Murphy.

References

Ammann, C., Brunner, A., Spirig, C. and Neftel, A.: Technical note: Water vapour concentration and flux measurements with PTR-MS, Atmos. Chem. Phys., 6, 4643–4651, 2006.

Aubinet, M., Vesala, T. and Papale, D.: Eddy Covariance: A Practical Guide to Measurement and Data Analysis, 2012., Springer Netherlands, Dordrecht. [online] Available from: http://dx.doi.org/10.1007/978-94-007-2351-1, 2012.

Baum, K. A. and Ham, J. M.: Adaptation of a speciation sampling cartridge for measuring ammonia flux from cattle feedlots using relaxed eddy accumulation, Atmos. Environ., 43(10), 1753–1759, doi:10.1016/j.atmosenv.2008.12.021, 2009.

Brodeur, J. J., Warland, J. S., Staebler, R. M. and Wagner-Riddle, C.: Technical note: Laboratory evaluation of a tunable diode laser system for eddy covariance measurements of ammonia flux, Agric. For. Meteorol., 149(2), 385–391, doi:10.1016/j.agrformet.2008.08.009, 2009.

Ellis, R. a., Murphy, J. G., Pattey, E., van Haarlem, R., O’Brien, J. M. and Herndon, S. C.: Characterizing a Quantum Cascade Tunable Infrared Laser Differential Absorption Spectrometer (QC-TILDAS) for measurements of atmospheric ammonia, Atmos. Meas. Tech., 3(2), 397–406, doi:10.5194/amt-3-397-2010, 2010.

Erisman, J. W., Galloway, J. N., Seitzinger, S. P., Bleeker, A., Dise, N. B., Petrescu, A. M. R., Leach, A. M. and de Vries, W.: Consequences of human modification of the global nitrogen cycle, Philos. Trans. R. Soc. B Biol. Sci., 368(1621), doi:10.1098/rstb.2013.0116, 2013.

Famulari, D., Fowler, D., Hargreaves, K., Milford, C., Nemitz, E., Sutton, M. a. and Weston, K.: Measuring Eddy Covariance Fluxes of Ammonia Using Tunable Diode Laser Absorption Spectroscopy, Water, Air, Soil Pollut. Focus, 4(6), 151–158, doi:10.1007/s11267-004-3025-1, 2004.

Famulari, D., Fowler, D., Nemitz, E., Hargreaves, K. J., Storeton-West, R. L., Rutherford, G., Tang, Y. S., Sutton, M. A. and Weston, K. J.: Development of a low-cost system for measuring conditional time-averaged gradients of SO2 and NH3, Environ. Monit. Assess., 161(1–4), 11–27, doi:10.1007/s10661-008-0723-6, 2010.

Ferrara, R. M., Loubet, B., Di Tommasi, P., Bertolini, T., Magliulo, V., Cellier, P., Eugster, W. and Rana, G.: Eddy covariance measurement of ammonia fluxes: Comparison of high frequency correction methodologies, Agric. For. Meteorol., 158–159, 30–42, doi:10.1016/j.agrformet.2012.02.001, 2012.

Ferrara, R. M., Carozzi, M., Di Tommasi, P., Nelson, D. D., Fratini, G., Bertolini, T., Magliulo, V., Acutis, M. and Rana, G.: Dynamics of ammonia volatilisation measured by eddy covariance during slurry spreading in north Italy, Agric. Ecosyst. Environ., 219, 1–13, doi:10.1016/j.agee.2015.12.002, 2016.

Finkelstein, P. L. and Sims, P. F.: Sampling error in eddy correlation flux measurements, J. Geophys. Res. Atmos., 106(D4), 3503–3509, doi:10.1029/2000JD900731, 2001.

Finnigan, J. J., Clement, R., Malhi, Y., Leuning, R. and Cleugh, H. A.: A re-evaluation of long-term flux measurement techniques - Part I: Averaging and coordinate rotation, Boundary-Layer Meteorol., 107(1), 1–48, doi:10.1023/a:1021554900225, 2003.

Flechard, C. R. and Fowler, D.: Atmospheric ammonia at a moorland site. II: Long-term surface-atmosphere micrometeorological flux measurements, Q. J. R. Meteorol. Soc., 124(547), 759–791, doi:10.1002/qj.49712454706, 1998.

Foken, T. and Wichura, B.: Tools for quality assessment of surface-based flux measurements, Agric. For. Meteorol., 78(1–2), 83–105, doi:10.1016/0168-1923(95)02248-1, 1996.

Foken, T., Leuning, R., Oncley, S., Mauder, M. and Aubinet, M.: Corrections and Data Quality Control, in Eddy Covariance, edited by M. Aubinet, T. Vesala, and D. Papale, pp. 85–131, Springer Netherlands., 2012.

Hansen, K., Sørensen, L. L., Hertel, O., Geels, C., Skjøth, C. A., Jensen, B. and Boegh, E.: Ammonia emissions from deciduous forest after leaf fall, Biogeosciences, 10(7), 4577–4589, doi:10.5194/bg-10-4577-2013, 2013.

Hansen, K., Pryor, S. C., Boegh, E., Hornsby, K. E. and Soerensen, L. L.: Background concentrations and fluxes of atmospheric ammonia over a deciduous forest, Agric. For. Meteorol., In review, 380–392, doi:10.1016/j.agrformet.2015.09.004, 2015.

Hensen, A., Nemitz, E., Flynn, M. J., Blatter, A., Jones, S. K., Sorensen, L. L., Hensen, B., Pryor, S. C., Jensen, B., Otjes, R. P., Cobussen, J., Loubet, B., Erisman, J. W., Gallagher, M. W., Neftel, A. and Sutton, M. A.: Inter-comparison of ammonia fluxes obtained using the Relaxed Eddy Accumulation technique, Biogeosciences, 6(11), 2575–2588, 2009.

Herndon, S. C., Zahniser, M. S., Nelson, D. D., Shorter, J., McManus, J. B., Jiménez, R., Warneke, C. and de Gouw, J. A.: Airborne measurements of HCHO and HCOOH during the New England Air Quality Study 2004 using a pulsed quantum cascade laser spectrometer, J. Geophys. Res., 112(D10), D10S03, doi:10.1029/2006JD007600, 2007.

Horst, T. W.: A simple formula for attenuation of eddy fluxes measured with first-order-response scalar sensors, Boundary-Layer Meteorol., 82(2), 219–233, 1997.

Ibrom, A., Dellwik, E., Flyvbjerg, H., Jensen, N. O. and Pilegaard, K.: Strong low-pass filtering effects on water vapour flux measurements with closed-path eddy correlation systems, Agric. For. Meteorol., 147, 140–156, 2007.

Kaimal, J. C. and Finnigan, J. J.: Atmospheric boundary layer flows: their structure and measurement, Oxford University Press., 1994.

Li, H., Cheng, J., Zhang, Q., Zheng, B., Zhang, Y., Zheng, G. and He, K.: Rapid transition in winter aerosol composition in Beijing from 2014 to 2017: response to clean air actions, Atmos. Chem. Phys. Discuss., doi:10.5194/acp-2019-450, 2019.

Massman, W. J. and Ibrom, A.: Attenuation of concentration fluctuations of water vapor and other trace gases in turbulent tube flow, Atmos. Chem. Phys., 8(20), 6245–6259, 2008.

Mauder, M., Cuntz, M., Drüe, C., Graf, A., Rebmann, C., Schmid, H. P., Schmidt, M. and Steinbrecher, R.: A strategy for quality and uncertainty assessment of long-term eddy-covariance measurements, Agric. For. Meteorol., 169(0), 122–135, doi:http://dx.doi.org/10.1016/j.agrformet.2012.09.006, 2013.

McManus, J. B., Zahniser, M. S., Nelson, Jr., D. D., Shorter, J. H., Herndon, S. and Wood, E.: Application of quantum cascade lasers to high-precision atmospheric trace gas measurements, Opt. Eng., 49(11), 111124, doi:10.1117/1.3498782, 2010.

Miller, D. J., Sun, K., Tao, L., Khan, M. a. and Zondlo, M. a.: Open-path, quantum cascade-laser-based sensor for high-resolution atmospheric ammonia measurements, Atmos. Meas. Tech., 7(1), 81–93, doi:10.5194/amt-7-81-2014, 2014.

Moore, C. J.: Frequency response corrections for eddy correlation systems, Boundary-Layer Meteorol., 37(1–2), 17–35, 1986.

Moravek, A., Trebs, I. and Foken, T.: Effect of imprecise lag time and high-frequency attenuation on surface-atmosphere exchange fluxes determined with the relaxed eddy accumulation method, J. Geophys. Res. Atmos., 118(17), 10210–10224, doi:10.1002/jgrd.50763, 2013.

Moravek, A., Foken, T. and Trebs, I.: Application of a GC-ECD for measurements of biosphere–atmosphere exchange fluxes of peroxyacetyl nitrate using the relaxed eddy accumulation and gradient method, Atmos. Meas. Tech. Discuss., 7(2), 1917–1974, doi:10.5194/amtd-7-1917-2014, 2014.

Moravek, A., Murphy, J. G., Hrdina, A., Lin, J. C., Pennell, C., Franchin, A., Middlebrook, A. M., Fibiger, D. L., Womack, C. C., McDuffie, E. E., Martin, R., Moore, K., Baasandorj, M. and Brown, S. S.: Wintertime Spatial Distribution of Ammonia and its Emission Sources in the Great Salt Lake Region, Atmos. Chem. Phys. Discuss., 2019, 1–28, doi:10.5194/acp-2019-266, 2019.

Myles, L., Meyers, T. P. and Robinson, L.: Relaxed eddy accumulation measurements of ammonia, nitric acid, sulfur dioxide and particulate sulfate dry deposition near Tampa, FL, USA, Environ. Res. Lett., 2(3), doi:10.1088/1748-9326/2/3/034004, 2007.

Nelson, A. J., Koloutsou-Vakakis, S., Rood, M. J., Myles, L., Lehmann, C., Bernacchi, C., Balasubramanian, S., Joo, E., Heuer, M., Vieira-Filho, M. and Lin, J.: Season-long ammonia flux measurements above fertilized corn in central Illinois, USA, using relaxed eddy accumulation, Agric. For. Meteorol., 239, 202–212, doi:10.1016/j.agrformet.2017.03.010, 2017.

Nelson, D. D., McManus, B., Urbanski, S., Herndon, S. and Zahniser, M. S.: High precision measurements of atmospheric nitrous oxide and methane using thermoelectrically cooled mid-infrared quantum cascade lasers and detectors, Spectrochim. Acta - Part A Mol. Biomol. Spectrosc., 60(14), 3325–3335, doi:10.1016/j.saa.2004.01.033, 2004.

Pan, Y., Tian, S., Liu, D., Fang, Y., Zhu, X., Zhang, Q., Zheng, B., Michalski, G. and Wang, Y.: Fossil Fuel Combustion-Related Emissions Dominate Atmospheric Ammonia Sources during Severe Haze Episodes: Evidence from 15N-Stable Isotope in Size-Resolved Aerosol Ammonium, Environ. Sci. Technol., doi:10.1021/acs.est.6b00634, 2016.

Pattey, E., Desjardins, R. L., Boudreau, F. and Rochette, P.: Impact of density-fluctuations on flux measurements of trace gases - implications for the relaxed eddy accumulation technique, Boundary-Layer Meteorol., 59(1–2), 195–203, doi:10.1007/bf00120695, 1992.

Pattey, E., Royds, W. G., Desjardins, R. L., Buckley, D. J. and Rochette, P.: Application software for a data acquisition and control system for measuring atmospheric trace gas and energy fluxes, Comput. Electron. Agric., 15(4), 303–321, doi:https://doi.org/10.1016/0168-1699(96)00023-3, 1996.

Pattey, E., Edwards, G., Strachan, I. B., Desjardins, R. L., Kaharabata, S. and Riddle, C. W.: Towards standards for measuring greenhouse gas fluxes from agricultural fields using instrumented towers, Can. J. Soil Sci., 86(3), 373–400, 2006.

Paulot, F., Jacob, D. J., Pinder, R. W., Bash, J. O., Travis, K. and Henze, D. K.: Ammonia emissions in the United States, european union, and China derived by high-resolution inversion of ammonium wet deposition data: Interpretation with a new agricultural emissions inventory (MASAGE_NH3), J. Geophys. Res., 119(7), 4343–4364, doi:10.1002/2013JD021130, 2014.

Pozzer, A., Tsimpidi, A. P., Karydis, V. a., de Meij, A. and Lelieveld, J.: Impact of agricultural emission reductions on fine particulate matter and public health, Atmos. Chem. Phys. Discuss., 1–19, doi:10.5194/acp-2017-390, 2017.

R Core Team: R: A Language and Environment for Statistical Computing, [online] Available from: https://www.r-project.org, 2017.

Roscioli, J. R., Zahniser, M. S., Nelson, D. D., Herndon, S. C. and Kolb, C. E.: New Approaches to Measuring Sticky Molecules: Improvement of Instrumental Response Times Using Active Passivation, J. Phys. Chem. A, 150624112729005, doi:10.1021/acs.jpca.5b04395, 2015.

Shaw, W. J., Spicer, C. W. and Kenny, D. V.: Eddy correlation fluxes of trace gases using a tandem mass spectrometer, Atmos.

Environ., 32(17), 2887–2898, doi:10.1016/S1352-2310(98)00036-3, 1998.

Sintermann, J., Spirig, C., Jordan, A., Kuhn, U., Ammann, C. and Neftel, A.: Eddy covariance flux measurements of ammonia by high temperature chemical ionisation mass spectrometry, Atmos. Meas. Tech., 4(3), 599–616, doi:10.5194/amt-4-599-2011, 2011.

Sun, K., Tao, L., Miller, D. J., Zondlo, M. a., Shonkwiler, K. B., Nash, C. and Ham, J. M.: Open-path eddy covariance measurements of ammonia fluxes from a beef cattle feedlot, Agric. For. Meteorol., 213, 193–202, doi:10.1016/j.agrformet.2015.06.007, 2015.

Sutton, M. a., Nemitz, E., Milford, C., Fowler, D., Moreno, J., San José, R., Wyers, G. P., Otjes, R. P., Harrison, R., Husted, S. and Schjoerring, J. K.: Micrometeorological measurements of net ammonia fluxes over oilseed rape during two vegetation periods, Agric. For. Meteorol., 105(4), 351–369, doi:10.1016/S0168-1923(00)00203-3, 2000.

Walker, J. T., Robarge, W. P., Wu, Y. and Meyers, T. P.: Measurement of bi-directional ammonia fluxes over soybean using the modified Bowen-ratio technique, Agric. For. Meteorol., 138(1–4), 54–68, doi:10.1016/j.agrformet.2006.03.011, 2006.

Webb, E. K., Pearman, G. I. and Leuning, R.: Correction of flux measurements for density effects due to heat and water vapour transfer, Q. J. R. Meteorol. Soc., 106(447), 85–100, doi:10.1002/qj.49710644707, 1980.

Whitehead, J. D., Twigg, M., Famulari, D., Nemitz, E., Sutton, M. A., Gallagher, M. W. and Fowler, D.: Evaluation of Laser Absorption Spectroscopic Techniques for Eddy Covariance Flux Measurements of Ammonia, Environ. Sci. Technol., 42(6), 2041–2046, doi:10.1021/es071596u, 2008.

Wilczak, J. M., Oncley, S. P. and Stage, S. A.: Sonic anemometer tilt correction algorithms, Boundary-Layer Meteorol., 99(1), 127–150, doi:10.1023/A:1018966204465, 2001.

Wolff, V., Trebs, I., Ammann, C. and Meixner, F. X.: Aerodynamic gradient measurements of the NH3-HNO3-NH4NO3 triad using a wet chemical instrument: an analysis of precision requirements and flux errors, Atmos. Meas. Tech., 3(1), 187–208, 2010.

Zhu, T., Pattey, E. and Desjardins, R. L.: Relaxed eddy-accumulation technique for measuring ammonia volatilization, Environ. Sci. Technol., 34(1), 199–203, doi:10.1021/es980928f, 2000.

Zhu, Z., Xin, H., Li, H. and Dong, H.: Assessment of tubing type on ammonia gas adsorption, Appl. Eng. Agric., 2012.

Zöll, U., Brümmer, C., Schrader, F., Ammann, C., Ibrom, A., Flechard, C. R., Nelson, D. D., Zahniser, M. and Kutsch, W. L.: Surface-atmosphere exchange of ammonia over peatland using QCL-based eddy-covariance measurements and inferential modeling, Atmos. Chem. Phys., 16(17), 11283–11299, doi:10.5194/acp-16-11283-2016, 2016.

Tables

Table 1: Statistics of the NH_3 flux quality control for the flux data collected over the 5 month experiment period. Values given in ng m^{-2} s^{-1} represent the median value for the period.

	valid flux data		quality control		NH_3 fluxes		random flux error		flux detection limit (LOD)	
			QC flag ≤ 3	QC flag ≤ 6	emission (QC flag ≤ 3)	deposition (QC flag ≤ 3)	instrumental (σ_{cov}^{noise})	stochastic (σ_{cov}^{stoch})	LOD = $2 \cdot \sigma_{cov}^{stoch}$	below LOD (QC flag ≤ 3)
	#	% of period	% of valid flux data	% of valid flux data	ng m^{-2} s^{-1}	ng m^{-2} s^{-1}	ng m^{-2} s^{-1}	ng m^{-2} s^{-1}	ng m^{-2} s^{-1}	%
total	**6089**	**85.6**	**56.8**	**88.8**	**6.27**	**-9.65**	**0.13**	**1.08**	**2.15**	**11.6**
day	3028	85.0	68.2	93.4	8.59	-19.87	0.17	1.61	3.23	9.4
night	3061	86.1	45.6	84.3	3.46	-4.27	0.08	0.72	1.43	14.9

Figures

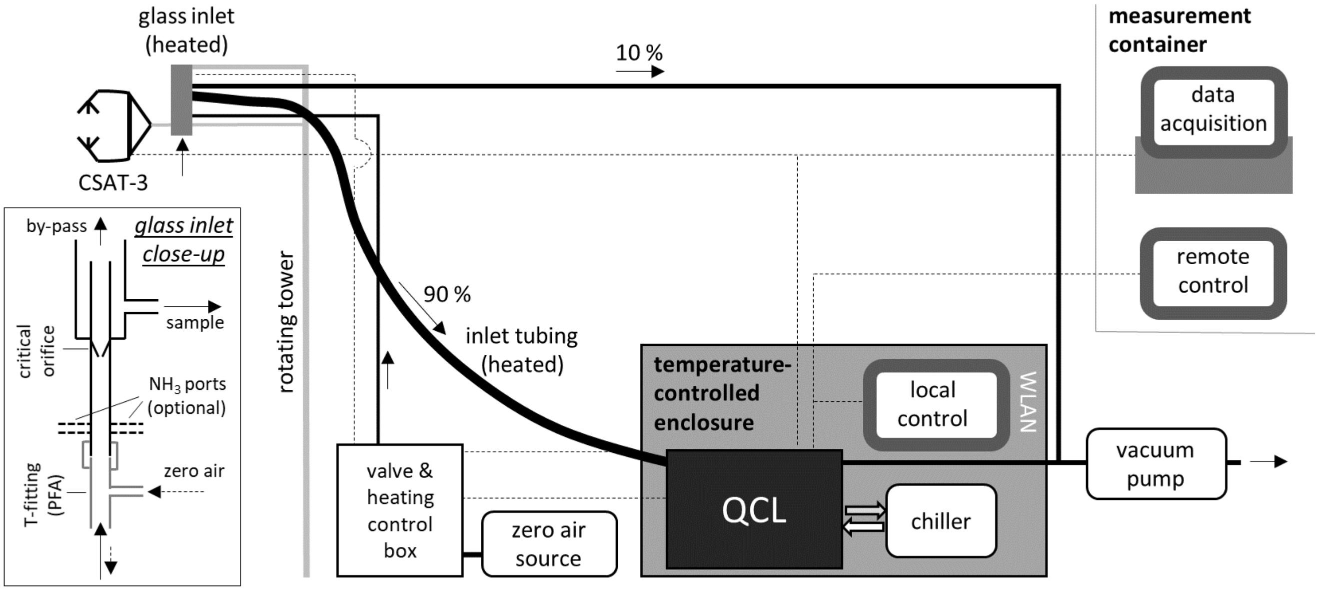

Figure 1: Schematic overview of the measurement setup. The glass inlet of the QCL is mounted next to the sonic anemometer (measurement height 2.5 m, later 4.5 m). Inside the glass inlet (see Ellis et al., 2010), a critical orifice reduces the pressure regime and a sharp turn of the flow path leads to a reduction of particulate matter. A heated sample tubing (length of 5.5 m) leads the sample air (flow rate of 13.4 to 15.4 L min^{-1}) to the QCL, which is housed in a temperature-humidity controlled enclosure. Dotted lines show electrical connections for data acquisition and control of the inlet heating and QCL analyser.

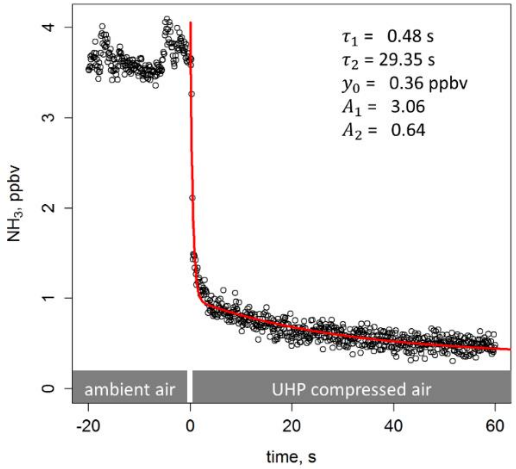

Figure 2: Time response of the 10 Hz NH_3 measurement. Shown is the step change NH_3 mixing ratios after switching from ambient air to the UHP compressed air. The red line is the fit of the double exponential decay function.

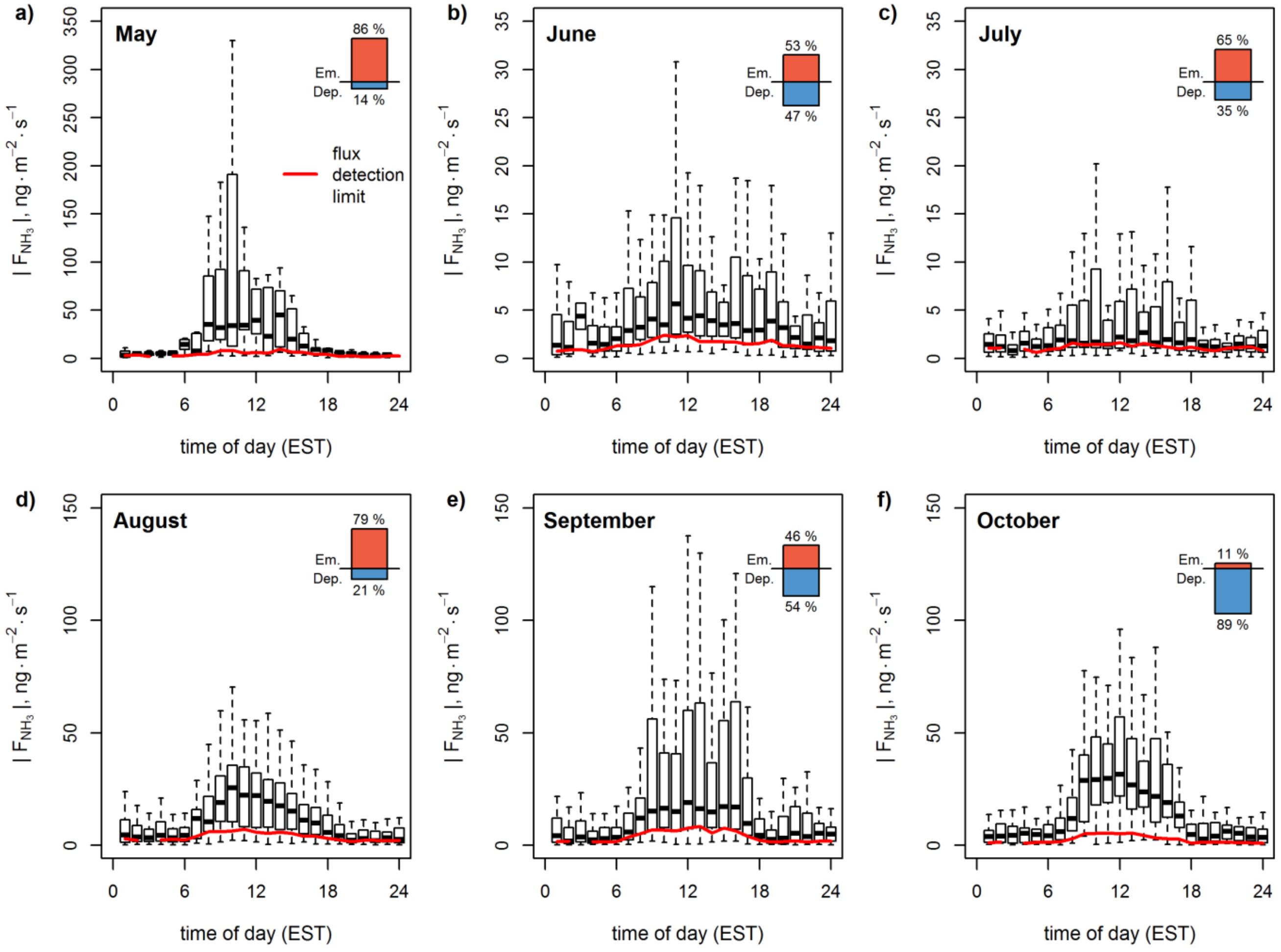

Figure 3: Boxplot statistics of diurnal absolute NH_3 fluxes for each month from May to October 2017 before the application of a HFA correction. Red lines illustrate the diurnal course of the median flux detection limit. ~~Shown fluxes are before the application of a HFA correction.~~ The percentages of flux periods with emission or deposition are indicated in the top right corner of each month.

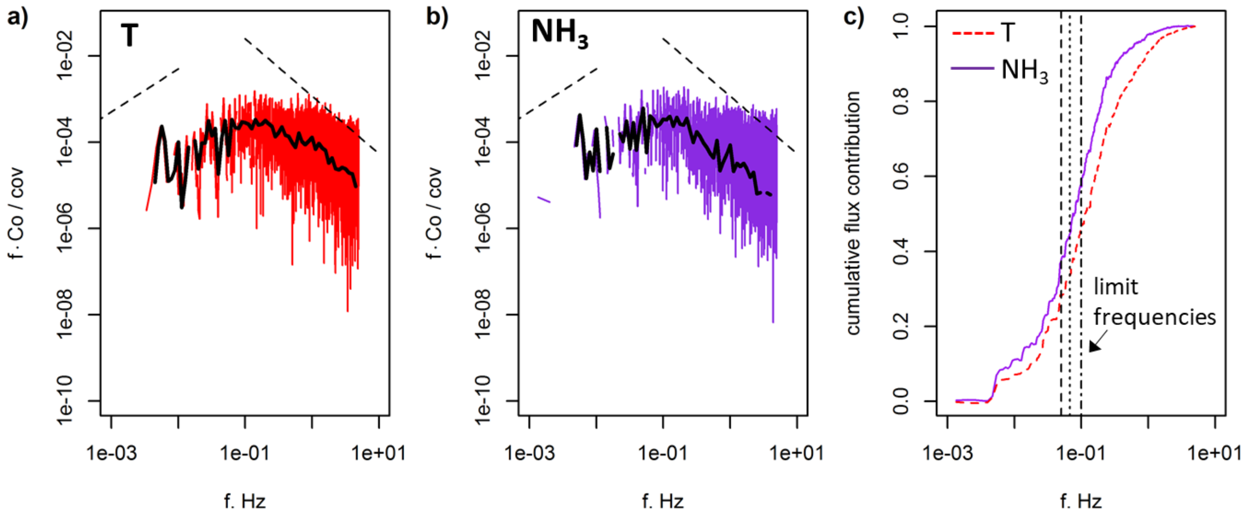

Figure 4: Results from the spectral analysis. (a) + (b) Shown are the co-spectral densities for the sensible heat and NH_3 flux for the period from 12:00 to 12:30 EST on 9 August 2017. The dash lines indicate the expected slopes in the low frequency range and the inertial subrange. c) The cumulative flux contribution (ogive) for both the sensible heat flux (T) and the NH_3 flux are shown for the same 30 min period. The dashed, dotted and dash-dotted vertical lines represent the limit frequencies used in the flux loss analysis at 0.05, 0.067 and 0.10 Hz, respectively.

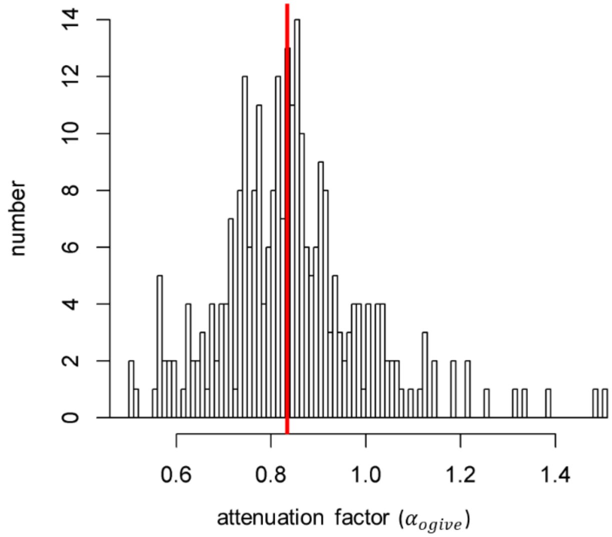

Figure 5: Results from the ogive analysis show the frequency distribution of the flux attenuation factor (α_{ogive}). Values lower than unity represent an underestimation of the NH_3 flux. The red vertical line marks the median value of 0.83 corresponding to a flux loss of 17 %.

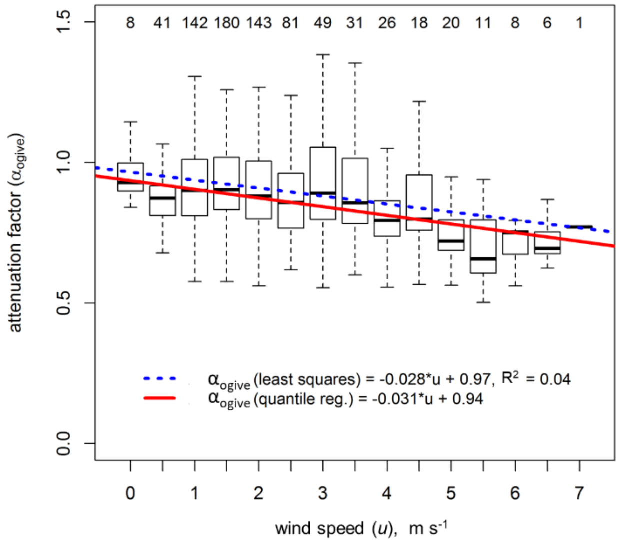

Figure 6: **Boxplot statistics of f~~F~~lux attenuation factors from the ogive analysis against the binned horizontal wind speed. Numbers on the top denote the number of data points in each bin. Both the least square and the quartile regression lines are shown. The coefficients from the quartile regression were used in Eq. 9.**

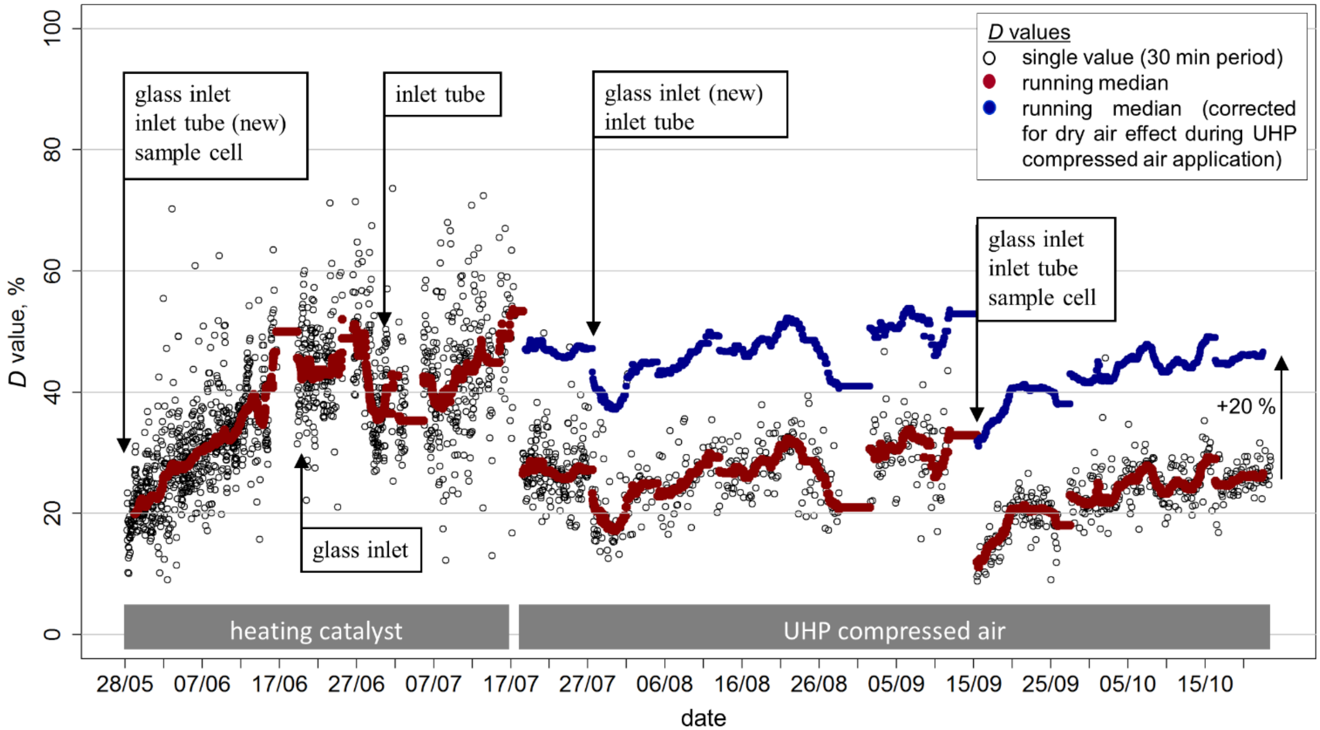

Figure 7: Variation in the time response during the experiment, represented by the *D* value, together with times of cleaning of the QCL inlet system. The *D* value gives the percentage contribution of time constants associated with wall interactions. Red data points represent the 48 hr moving median *D* value. To correct for the effect of dry air on the times response, the *D* values during times when the UHP compressed air was operated were increased by 20 % (blue data points).

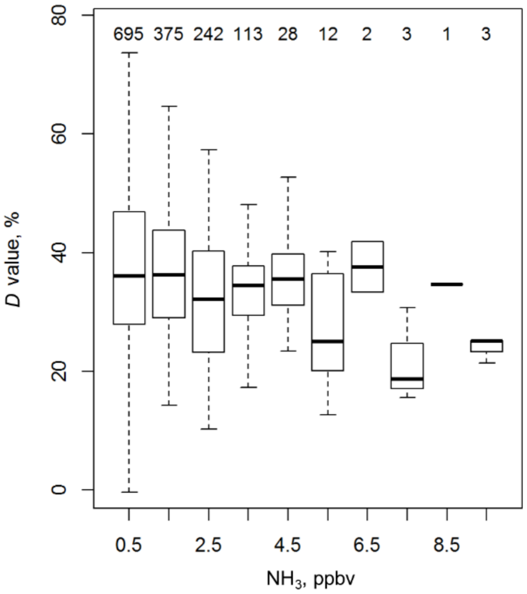

Figure 8: Boxplots statistics of time response results: *D* values against the binned ambient NH$_3$ mixing ratios before switching to the zero air source. Numbers on the top denote the number of data points in each bin.

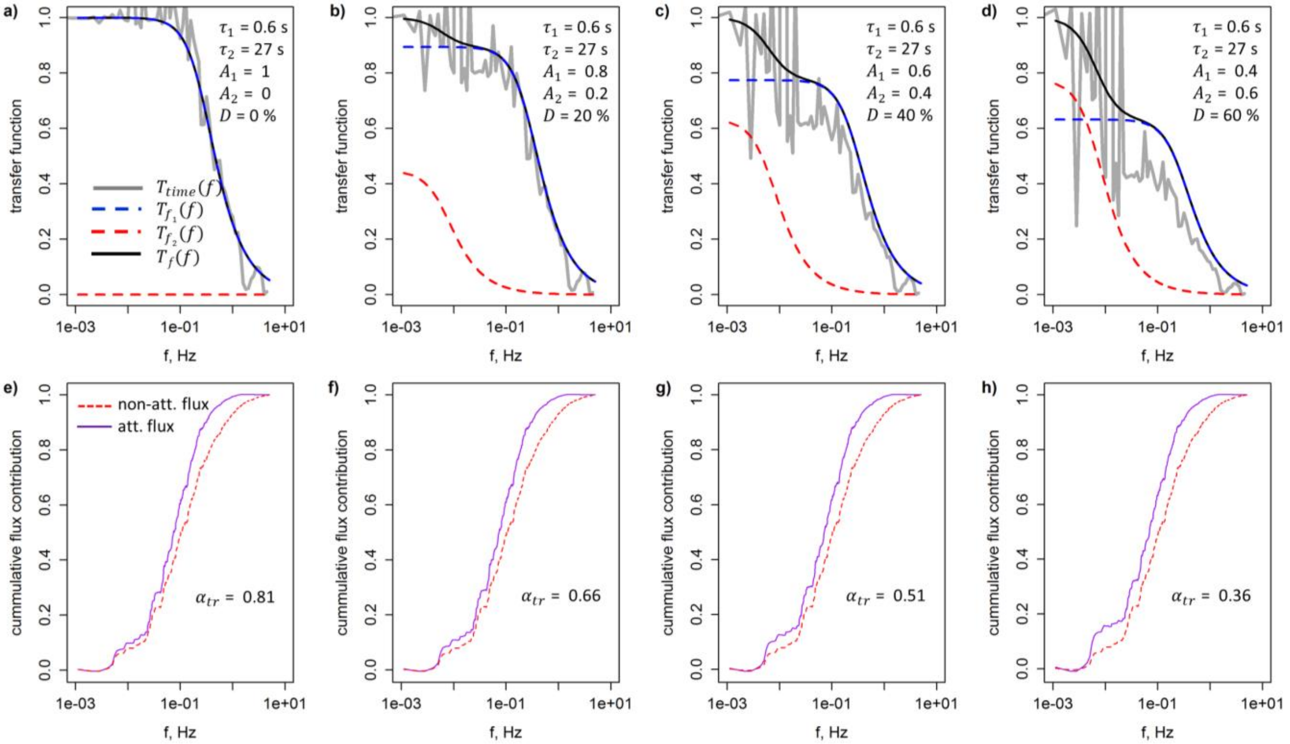

Figure 9: Results from the high frequency loss simulation shown for the period from 12:00 to 12:30 EST on 9 August 2017. a) - d): Calculated transfer functions for four different scenarios of *D* (= 0, 20, 40, 60 %) values from the time response fitting procedure.

Shown are~~-~~ the transfer function used in this study ($T_{\text{time}}(f)$), where the high frequency time series was low-pass filtered in the time domain, ~~(1)~~and the frequency domain transfer functions ($T_{f_1}(f)$) and ($T_{f_2}(f)$), which illustrate the flux loss associated with τ_1 and τ_2, respectively. Since the frequency domain transfer functions used here only account for the attenuation of the signal amplitudes and not the phase shift, their sum ($T_f(f)$) underestimates the flux loss compared to the time domain low-pass filter approach used in this study.~~ for the fast time response associated with the exchange of air volume in the QCL inlet system ($T_1(f)$), (2) the transfer function for the slow time response associated with wall interactions ($T_2(f)$), and (3) the combined transfer function ($T(f)$).~~ e) - f): The cumulative flux contribution (ogive) for the non-attenuated and attenuated sensible heat flux and calculated flux attenuation factors (α_{tr})~~ for the period from 12:00 to 12:30 EST on 9 August 2017 ~~. For each scenario the respective ~~combined~~ transfer function $T_{\text{time}}(f)$ in the panel above was used~~ to filter the temperature signal~~.

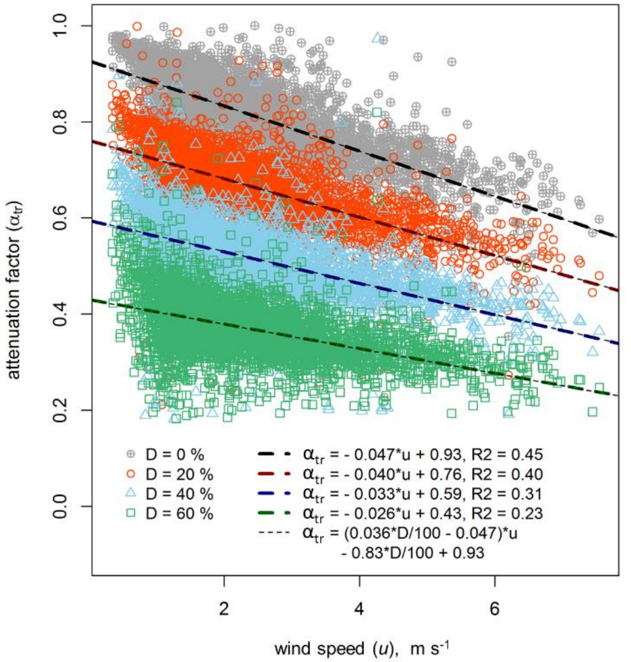

Figure 10: Correlation of the flux attenuation with horizontal wind speed for the different low-pass filter scenarios. The simulation was performed for all 30 min periods of the experiment, while for each scenario a linear regression function was derived. The four light dashed lines show the general fitting function using the *D* values from the simulation (Eq. ~~10~~12).

Supplementary Material for:

Measurements and quality control of ammonia eddy covariance fluxes: A new strategy for high frequency attenuation correction

Alexander Moravek[1*], Saumya Singh[1], Elizabeth Pattey[2], Luc Pelletier[2], Jennifer G. Murphy[1]

[1]Department of Chemistry, University of Toronto, Toronto, ON, M5S 3H6, Canada
[2]Agriculture and Agri-Food Canada, Ottawa, ON, K1A 0C6, Canada
*now at: Department of Chemistry, York University, Toronto, ON, M3J 1P3, Canada

Content:

WindTrax simulation

The range of possible NH3 fluxes during the peak emission periods after fertilization was investigated using WindTrax (Thunder Beach Scientific, Canada). WindTrax uses backward Lagrangian Stochastic (bLS) modelling to inferred flux estimates based on the measured trace gas mixing ratios and information on the turbulent transport. For the approach, the background mixing ratio has to be known and the source area (in case of emission) has to be defined.

As input we used the NH_3 mixing ratio measured by the QCL and the turbulence statistics by the CSAT3 sonic anemometer at 2.5 m a.g.l. For practicability reasons, we defined the NH_3 source area as a circle with 500 m diameter centred at the measurement location, which approximately represents the average extent of the agricultural field in each wind direction. Since no background NH_3 measurements were made, which are needed for the flux calculation with WindTrax, we used in different scenarios a NH_3 background mixing ratio between 0 and 4 ppbv. For the analysis, we focused on two days with the highest emission fluxes, 28 and 30 May 2017 (8:00 – 16:00), where the background NH_3 would be expected to have less influence on the NH_3 mixing ratio from QCL than during other conditions.

As shown in Fig. S1, on 28 May NH_3 mixing ratios ranged from 2.7 to 10.2 ppbv, with the peak mixing ratio measured at 10:30 EST. At that time also the highest NH3 emission flux of 753 ng m^{-2} s^{-1} was observed, indicating that a significant fraction of the measured NH_3 mixing ratio is linked to the emission from the fertilized corn field. Assuming a background mixing ratio of 2 ppbv, which seems a realistic background value given night time NH_3 mixing ratios of about 2 ppbv during that period, the modelled flux using WindTrax is with 829 ng m^{-2} s^{-1} very close to the measured NH_3 flux. Assuming a background mixing ratio of 0 ppbv, which represents the upper limit of possible NH_3 emissions modelled with WindTrax, yields an emission flux of 1034 ng m^{-2} s^{-1} at that time. The 30 min periods before and after the peak show the best match between modelled and measured NH_3 fluxes for NH_3 backgrounds between 2 and 4 ppbv.

On 30 May, the prevailing NH_3 mixing ratios were lower and steadily between 2 and 3 ppbv. Still, the second highest NH_3 emission after fertilizer application was observed on that day, with a peak emission of 190 ng m^{-2} s^{-1} at 14:00 EST. This emission flux matches well with the modelled NH_3 flux of 193 ng m^{-2} s^{-1} at using a background of 2 ppbv. Under a background scenario of 0 ppbv, the maximal emission from WindTrax at that time period is 295 ng m^{-2} s^{-1}, which is 1.5 times larger than the measured flux.

The analysis with WindTrax, using the two days with the highest NH_3 emissions after fertilization, shows that the expected fluxes are in the range of the measured NH_3 fluxes during those periods. During the peak emissions on both days, the maximal WindTrax emission estimates are about 1.5 times higher than the fluxes measured by the eddy covariance system. Since no background measurements outside of the corn field domain are available, WindTrax could not be used for other periods of the dataset, where the NH_3 emission fluxes were smaller or even deposition was measured.

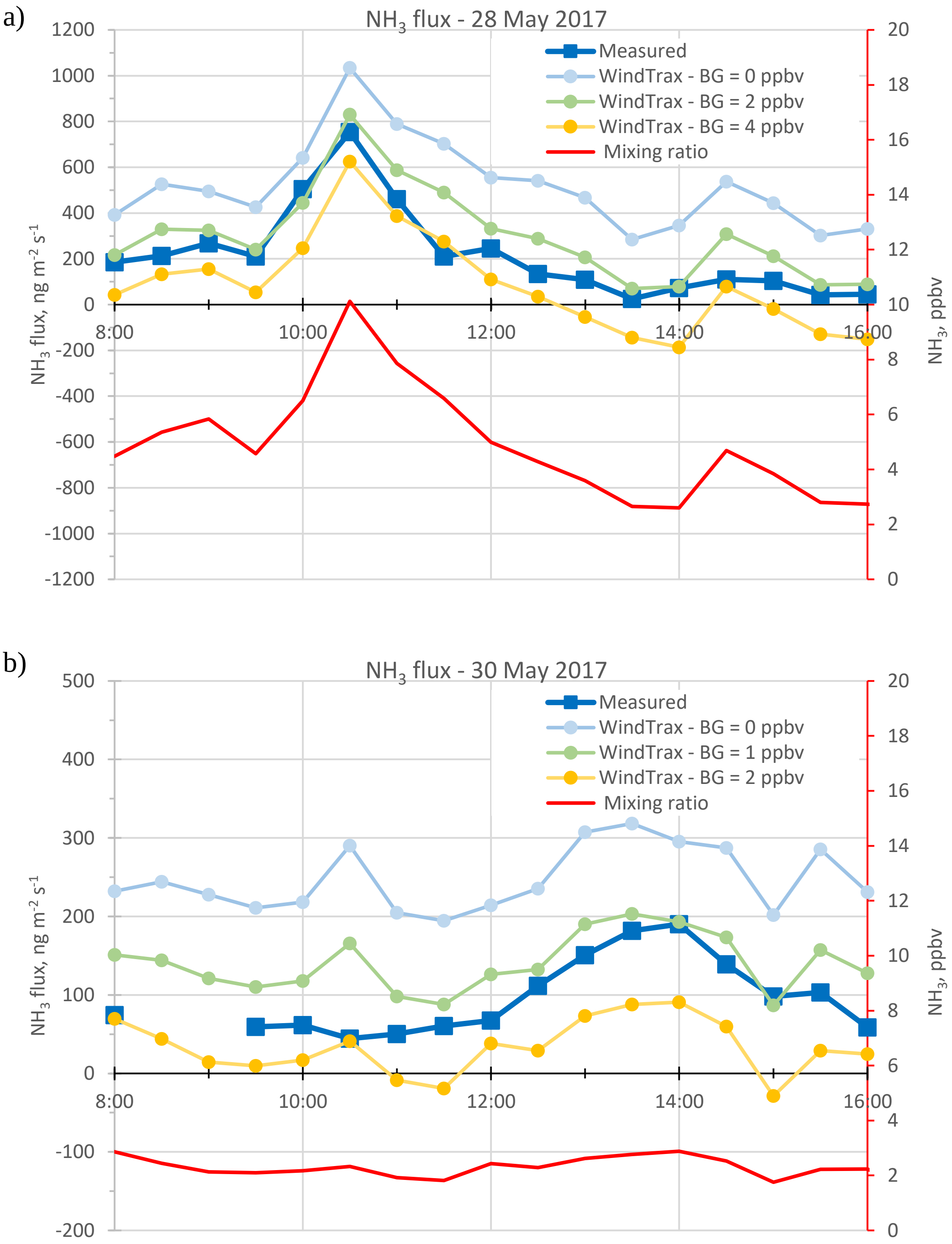

Figure S1: Estimated NH_3 fluxes from corn field using the WindTrax dispersion model. Shown are the daytime (8:00 to 16:00 EST) periods of (a) 28 May and (b) 30 May 2017, which were the periods when the highest NH_3 fluxes were measured. For the model estimates, scenarios with background NH_3 mixing ratios ranging from 0 to 4 ppbv were used. The measured eddy covariance fluxes, to which the results from the WindTrax model are compared, include the high frequency attenuation correction using the time response method.